Edith Cowan University

Research Online

Research outputs 2022 to 2026

6-1-2023

Influence of organics and gas mixing on hydrogen/brine and methane/brine wettability using Jordanian oil shale rocks: Implications for hydrogen geological storage

Amer Alanazi

Nurudeen Yekeen
Edith Cowan University, n.yekeen@ecu.edu.au

Mujahid Ali
Edith Cowan University, mujahid.ali@ecu.edu.au

Muhammad Ali
Edith Cowan University, m.ali@ecu.edu.au

Israa S. Abu-Mahfouz

See next page for additional authors

Follow this and additional works at: https://ro.ecu.edu.au/ecuworks2022-2026

 Part of the Engineering Commons

10.1016/j.est.2023.106865
Alanazi, A., Yekeen, N., Ali, M., Ali, M., Abu-Mahfouz, I. S., Keshavarz, A., ... & Hoteit, H. (2023). Influence of organics and gas mixing on hydrogen/brine and methane/brine wettability using Jordanian oil shale rocks: Implications for hydrogen geological storage. *Journal of Energy Storage*, 62, Article 106865.
https://doi.org/10.1016/j.est.2023.106865
This Journal Article is posted at Research Online.
https://ro.ecu.edu.au/ecuworks2022-2026/2016

Authors

Amer Alanazi, Nurudeen Yekeen, Mujahid Ali, Muhammad Ali, Israa S. Abu-Mahfouz, Alireza Keshavarz, Stefan Iglauer, and Hussein Hoteit

This journal article is available at Research Online: https://ro.ecu.edu.au/ecuworks2022-2026/2016

Journal of Energy Storage 62 (2023) 106865

Contents lists available at ScienceDirect

Journal of Energy Storage

journal homepage: www.elsevier.com/locate/est

Research papers

Influence of organics and gas mixing on hydrogen/brine and methane/brine wettability using Jordanian oil shale rocks: Implications for hydrogen geological storage

Amer Alanazi [a,*], Nurudeen Yekeen [b], Mujahid Ali [b], Muhammad Ali [a,b], Israa S. Abu-Mahfouz [c], Alireza Keshavarz [b], Stefan Iglauer [b], Hussein Hoteit [a]

[a] Physical Science and Engineering Division, King Abdullah University of Science and Technology (KAUST), Thuwal 23955, Saudi Arabia
[b] Petroleum Engineering Discipline, School of Engineering, Edith Cowan University, 270 Joondalup Dr., Joondalup 6027, WA, Australia
[c] Department of Petroleum Engineering and Geosciences, King Fahd University of Petroleum and Minerals, Dhahran 31261, Saudi Arabia

ARTICLE INFO

Keywords:
Jordanian oil shale
Organic acids
Wettability
Hydrogen
Geological storage
Gas mixing

ABSTRACT

The substitution of fossil fuel with clean hydrogen (H_2) has been identified as a promising route to achieve net zero carbon emissions by this century. However, enough H_2 must be stored underground at an industrial scale to achieve this objective due to the low volumetric energy density of H_2. In underground H_2 storage, cushion gases, such as methane (CH_4), are required to maintain a safe operational formation pressure during the withdrawal or injection of H_2. The wetting characteristics of geological formations in the presence of H_2, cushion gas, and the resultant gas mixture in the mixing zone between them are essential for determining storage capacities. Therefore, the present work measured the contact angles of four Jordanian oil shale rocks with H_2, CH_4, and H_2-CH_4/brine mixture systems and their interfacial tension (IFT) in geological storage (geo-storage) conditions (pressures of 0.1 to 1600 psi and temperature at 323 K) to evaluate the residual and structural trapping potential and efficiency of CH_4 as a cushion gas. Various analytical methods were employed to comprehend the bulk mineralogy, elemental composition, topographic characterization, functional groups, and surface properties of the Jordanian oil shale rocks. The total organic carbon (TOC) effect on wettability was demonstrated and compared with previous studies. The Jordanian oil shale samples with high to ultrahigh TOC of 13 % to 18 % exhibited high brine advancing/receding contact angles. The rock samples became hydrophobic at the highest experimental pressure and temperature conditions (1600 psi and 323 K). The rock/CH_4/brine contact angles were higher than the rock/H_2/brine contact angles, and the H_2-CH_4/brine mixture contact angles remained in between those for pure gases. Moreover, the IFT displayed the inverse trend, where the H_2/brine IFT measured higher than the CH_4/brine IFT. The results suggest that the H_2 geo-storage in the tested organic-rich source rocks could be favorable when CH_4 is used as a cushion gas, consistent with previous studies using synthetically acid-aged shale samples. For the first time, the present work used organic-rich rocks from Jordanian oil shale to present a more realistic situation and evaluate the influence of missing organic material and gas on the H_2/brine/rock wettability during H_2 geo-storage.

1. Introduction

The global energy demand could increase by >27 % within the next three decades as the world population attains the 10 billion mark, increased from 7.98 billion [1–3]. The world has relied on fossil fuels as the primary energy source for centuries [4,5]. Burning fossil fuels remains the primary source of anthropogenic carbon dioxide (CO_2) emissions, a principal greenhouse gas contributing to global warming and increasing the earth's temperature [3,6,7]. With the increasing global ambition to achieve net zero carbon emissions by midcentury [8,9], reducing the continual reliance on fossil fuels while maintaining a balance between energy supply and increasing energy demand is essential [10–13].

Renewable energy, such as solar, hydropower, and wind energy, is more sustainable and eco-friendlier than fossil fuels. However, their sources are intermittent and constrained to the earth's seasonal and

* Corresponding author.
E-mail address: Amer.alanazi@kaust.edu.sa (A. Alanazi).

https://doi.org/10.1016/j.est.2023.106865
Received 27 December 2022; Received in revised form 3 February 2023; Accepted 6 February 2023
Available online 15 February 2023
2352-152X/© 2023 The Author(s). Published by Elsevier Ltd. This is an open access article under the CC BY license (http://creativecommons.org/licenses/by/4.0/).

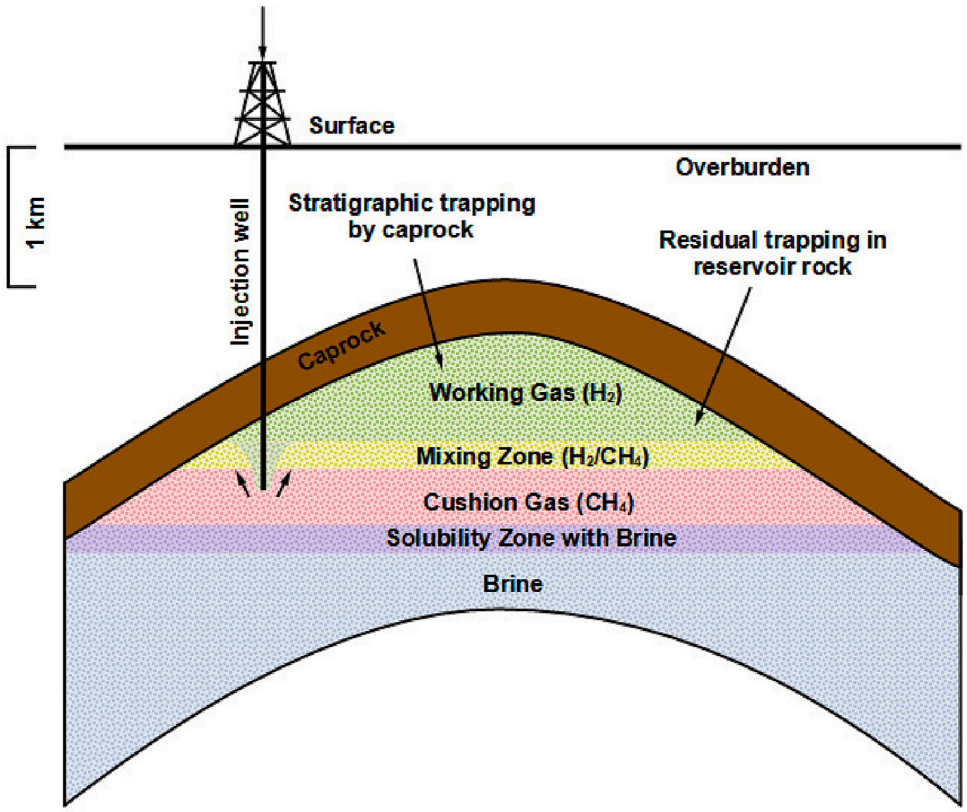

Fig. 1. Illustration of underground hydrogen storage and mixing zone between working gas (H_2) and cushion gas (CH_4).

quotidian cycles [14,15]. Recently, global attention has been focused on decarbonizing the industrial sectors via the hydrogen (H_2) economy [16–20] because it does not produce CO_2 when it burns and has low environmental and societal effects (a CO_2-free global economy) [17,21,22].

In contrast, H_2 has low volumetric energy content due to its low density. Consequently, substantial volumes of H_2 must be stored at an industrial scale to back up the H_2 supply when needed [23]. Underground H_2 storage (UHS) is perceived as an economical and safer option than surface storage facilities [20,24], which are challenging and costly to construct and maintain [25].

Currently, the only used UHS media are salt caverns, which are more straightforward than porous formations and do not cause the microbial consumption of H_2 [16,26–28]. Despite the complexity of porous formations, deep saline aquifers and depleted hydrocarbon reservoirs provide more spacious storage options. Their features are well known from the experience acquired from subsurface storage of natural gas and CO_2 for decades [29–33]. Similarly, the subsurface facilities previously used for the transportation and storage of hydrocarbons could be upgraded for H_2 storage and production [19,34].

Currently, the only known information on the possibility of UHS is deduced from experience with CO_2 and methane (CH_4) subsurface storage [33,35–37]. However, the characteristics of pure H_2 differ from those of CO_2 and CH_4 [38]. Hydrogen is the lightest known molecule in nature and has a considerably lower density than other gases [17,39]. Moreover, CO_2 is intended to be stored permanently in geological storage (geo-storage) formations, whereas H_2 is stored temporarily to be withdrawn during acute energy demands [11,16]. Formation pressure should be sustained using cushion gases to maintain the integrity of the reservoir during H_2 withdrawal [40–42]. Both CO_2 and CH_4 are possible cushion gases for H_2 withdrawal. However, these gases create a mixing zone between the stored gas (H_2) and cushion gases (CO_2 or CH_4) [33,43], as illustrated in Fig. 1.

Previously, a few studies have reported insight into the rock-brine-H_2 interaction and rock-fluid interfacial tension (IFT) [33,44–50]. The influences of subsurface temperature, pressure, salinity, and organic-acid contamination inherent in geo-storage/caprock formations have been investigated concerning their wetting characteristics and IFT interactions in the presence of H_2, CH_4, and CO_2 [33,35,42,51,52]. From these results, we inferred that the residual/capillary trapping of H_2 in storage rocks, such as sandstone/quartz and carbonate/calcite, and adsorption trapping in coal and high total organic carbon (TOC) shale could be lower at high temperatures and low pressures. Likewise, the structural trapping potential of caprock was surmised to be favorable at high temperatures and low pressures and in the absence of organic acids in an overlying seal [53–57].

Recently, Hashemi et al. [33] measured the static contact angles of H_2–CH_4/brine/Bentheimer sandstone systems to assess the mixed-zone, cushion, and working gas wettability and IFT. They found that the contact angles varied from 25° to 45° at geo-storage temperatures (30 °C and 50 °C) and pressures (20–100 bar). Their results further demonstrated that the wetting behavior of Bentheimer rock was similar in the presence of H_2, CH_4, and the H_2–CH_4 mixture regardless of the varying H_2 composition, geo-storage conditions, and sodium chloride (NaCl) concentrations.

Similarly, Mirchi et al. [43] computed the IFT values (via the pendant drop technique) and static contact angles for H_2-CH_4/brine on limestone and oil-wet sandstone at 1000 psi and 22 °C–60 °C using captive/rising bubble methods. The results revealed that the IFT decreased with rising temperatures and reducing H_2 fractions in the H_2–CH_4 mixture. The mixed system of H_2 and potential cushion gas (CH_4) demonstrated similar weakly water-wet characteristics on limestone and oil-wet sandstone rocks. Moreover, the contact angles varied from 52.42° to 71.1°. In addition, the contact angles of the H_2/brine systems on the rock surfaces were lower than those of the CH_4/brine systems, suggesting that CH_4 could be a feasible (promising) cushion gas for H_2 storage and withdrawal.

Van Rooijen et al. [58] confirmed that the storage media could

Table 1
Summary of selected previous research reporting the contact angles of rock/H_2/brine systems.

Samples	Methodology	Temperature	Pressure	References	Remarks
Quartz	Captive bubble,	298 K	0.69–1.72 MPa & 6.89–20.68 MPa	Higgs et al. [69]	Effective contact angles of H_2/2000 ppm NaCl varied 31°–29° within a pressure range of 0.69–1.72 MPa, those of H_2/5000 ppm NaCl varied 35°–33° at 0.69–1.72 MPa, and the contact angle of H_2/water was 27° at 0.77 and 0.86 MPa
Bituminous coal	Tilted drop method	25 °C, 50 °C, and 70 °C	20–100 bar	Sedev et al. [70]	1. The coal surface was weakly water-wet in geo-storage 2. Brine contact angles increased with H_2 pressure at 25 °C, with no significant pressure effect on contact angles at 50 °C or 70 °C
Saudi basaltic rocks	Modified sessile drop method	323 K	3–28 MPa	Alanazi et al. [71]	1. Saudi basalt with −OH bonds and a higher Si-O-Si group had superior sealing potential for H_2 storage 2. Basaltic rocks with smaller pore sizes have higher storage potential
Sandstone (oil-wet) and limestone	Rising/captive bubble method	22 °C–60 °C	100 psi	Mirchi et al. [43]	Contact angle values ranged from 52.42°–71.1°, suggesting that oil-wet sandstone and limestone remained weakly water-wet in the presence of an H_2/CH_4 mixture
Quartz	Experimental (tilted plate)	296 K–343 K	0.1–25 MPa	Iglauer et al. [50]	Contact angle values increased with pressure, temperature, and increased concentrations of organic acid
Mica	Experimental (tilted plate)	323 K	0.1–25 MPa	Ali et al. [59]	Advancing and receding contact angle values reached 106.2° and 97.3° when mica was aged in 10^{-2} mol/L of organic-acid/n-decane solution at 323 K and 25 MPa
Clay minerals	Empirical correlations	333 K	5–20 MPa	Al-Yaseri et al. [72]	1. Contact angles were generally <40° 2. Montmorillonite was the most water-wet, whereas kaolinite was the least water-wet
Basalt	Empirical correlations	323 K	5–20 MPa	Al-Yaseri and Jha [47]	Contact angle values were generally < 20°
Sandstones (Berea and Bentheimer)	Experimental (captive bubble)	20 °C–50 °C	20–100 bar	Hashemi et al. [48]	Contact angle values vary between 25° and 45°
Quartz	Experimental (tilted plate)	323 K	0.1–25 MPa	Ali et al. [29]	Contact angle values were >90° when the effects of organic contamination (10^{-2} mol/L lignoceric acid) were considered
Shale	Tilted plate	298 K–353 K	0.1–20 MPa	Hosseini et al. [56]	Caprock became less water-wet at low temperatures, high pressures, higher TOC values, and increasing concentrations of organic acid
Shale (0.081–23.4 wt%)	Semi-empirical correlations	343 K	5–20 MPa	Al-Yaseri et al. [73]	Capillary entry pressure reduced, whereas contact angles increased with increasing pressure (depth) and the TOC of the shale
Berea sandstone (length = 17 cm; diameter = 3.8)	Combination of MICP data and capillary pressure	18 °C	100 bar	Boon and Hajibeygi [74]	1. The receding contact angle of the H_2/water system on a Berea sandstone rock core was estimated as 45° 2. Displacement patterns during UHS can result from the interplay between the capillarity and viscous and gravitational forces
Glass	Microfluidic chip	20 °C	10 bar	van Rooijen et al. [75]	1. The porous medium stayed strongly water-wet in H_2; dynamic advancing contact angles ranged from 13°–39°, whereas dynamic receding contact angles ranged from 6°–23° 2. Contact angle datasets of H_2, nitrogen, and gaseous CO_2 were comparable, and higher channel widths produced smaller contact angles
Quartz	Geochemical modeling	296 K, 323 K, 343 K	0.1–25 MPa	Zeng et al. [76]	1. Concentrations of quartz surface species (> SiO^- and > $SiOCa^+$) decreased with increased temperatures 2. No significant effect of increasing pressure and temperature was found on the disjoining pressure and H_2 wettability of pure quartz, but increasing pressure and concentrations of organic acid molecules increased the rock hydrophobicity and H_2-wettability of aged quartz

*MICP: mercury injection capillary pressure.

remain at water-wet conditions by measuring the contact angles of H_2/water on a microfluidic chip (with microchannel widths ranging from 50 to 130 m) at 20 °C and 10 bar. The microfluidic chip was completely saturated with water before H_2 injection for the drainage tests, whereas in the imbibition experiments, the microfluidic chip was entirely saturated with H_2 before water injection. The results revealed that the wetting state remained at strong water-wet conditions and that the H_2/water advancing contact angles varied between 13° and 39°, whereas the receding contact angles varied between 6° and 23°. These results confirmed that a fully H_2-wet state is difficult to attain during UHS.

In contrast, Ali et al. found that containment safety of H_2 in storage and caprock is overpredicted when the influence of organic impurities (contaminations), which are characteristic of natural geo-storage formations, is neglected and that fully H_2-wet conditions (contact angles> 90^o) can be attained in the presence of organic acids. Ali et al. [59] found that the caprock representative mineral (mica) demonstrated entirely H_2-wet behavior at 383 K and 25 MPa (θ_a= 106.2°, θ_r= 97.3°) in the presence of 10^{-2} mol/L of lignoceric acid. The rock hydrophobicity increased with an increased organic-acid concentration and alkyl chain length, as follows: hexanoic acid <lauric acid <lignoceric acid from C_6 to C_{24} [29,53,59,60]. The high values of standard adsorption energy promoted the interactions between rock surfaces and H_2 molecules, which increased with the increasing alkyl chain length of the organic acids. Generally, organic contamination and salinity reduce the storage rock potential and containment security of H_2.

Pan et al. [61] and Arif et al. [62] demonstrated that the contact angle increases when the TOC of shale samples increases from 2 % to 20 % at a temperature of 323 K. A summary of previous studies on rock/H_2/brine systems of storage/caprock is presented in Table 1. Only a few of these studies have provided insight into the rock-wetting phenomenon and rock-fluid IFT of the mixing zone between the stored gas and cushion gas during UHS in organic-rich shale source rocks [33,43]. Moreover, in most previous studies, the clean rock substrates were aged in organic acids, such as stearic and lignoceric acid, to assess the effects of organic contamination inherent in geo-storage formations. None of the previous studies have used the original source rock with inherent

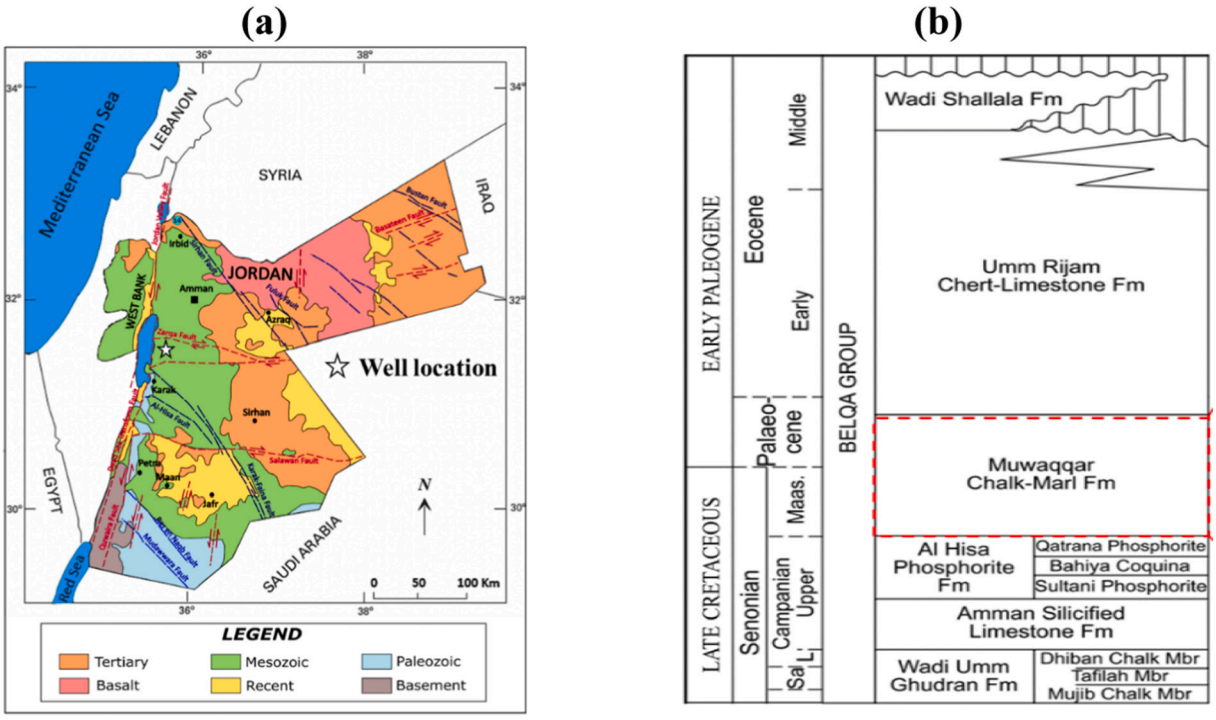

Fig. 2. (a) Geological map of Jordan marking the drilled well location and (b) generalized stratigraphic column with significant occurrences of Jordan shale source rocks from the Late Cretaceous to Early Paleogene (adapted from [79,80]).

organic-acid content to assess the effects of organic-acid contamination on the H_2-CH_4/brine/rock wettability and H_2-CH_4/brine IFT at geo-storage temperatures and pressures.

Thus, the present work evaluated the wettability and IFT of the H_2, CH_4, and H_2-CH_4 mixture (50 %/50 %) at 323 K at various pressures (0.1–1600 psi). A source rock, which is a good candidate for H_2 storage and inherently contains organic acids, was used as the rock substrate for the wettability measurement. Natural organic-rich shale source rocks (high TOC) from Jordan were used as rock substrates to evaluate the effects of natural organics on H_2, CH_4, and H_2-CH_4 mixture wettability. This work provides an understanding of the mixing-zone wettability and gas/brine IFT during UHS in organic-rich shale source rocks (Fig. 1). Several researchers have identified TOC to be a critical influencing parameter on the adsorption-desorption capacity and the storability of gas in calcareous and argillaceous source rocks [63–68]. Thus, this study also demonstrates the influence of organic material on the wettability and storability of H_2, CH_4, and the H_2-CH_4 mixture in these formations. The work provides a fundamental concept for UHS concerning organic matter and aids in implementing a large-scale H_2 economy for Jordanian oil shale rocks.

2. Materials and methods

2.1. Materials

The tested organic-rich shale source rocks, known as Jordanian oil shale, were collected from Jordan. The Jordanian oil shale rocks correspond to the Muwaqqar Chalk-Marl formation, deposited during the Late Cretaceous to Early Paleocene period [77]. The Jordanian oil shale source rocks are among the richest globally [78,79], with a TOC value as high as 30 %. However, these source rocks are thermally immature and have not been reported to produce hydrocarbons on an economic scale.

Four samples of Jordanian shale source rocks were selected at various depths from a well drilled in northwest Jordan (Fig. 2(a)). The organic-rich interval, corresponding to these litho-stratigraphic units, was deposited in reducing conditions with restricted water circulation and was characterized as Type II-IIS kerogen (Abed and Amireh, 1983; Hakimi et al., 2016; Powell and Moh'D, 2011) (Fig. 2b). The CH_4, H_2, and H_2-CH_4 mixture used for the experiments were of high purity (99.99 mol%, supplied from Coregas, Australia). The brine salinity of 2 wt% of NaCl with 1 wt% of potassium chloride (KCl) was used throughout the experiments. The NaCl and KCl were reagent grade (99.9 % pure, supplied by Chemlab, Australia).

2.2. Total organic carbon determination of Jordanian oil shale samples

The selected rock samples were powdered, and about 50 mg of each sample was analyzed using RockEval 7S (©Vinci Technologies) for TOC measurements. The methodological and assessment criteria have been described in previous research (Behar et al., 2001; Carvajal-Ortiz et al., 2021). The parameters obtained from this analysis include S1, S2, S3, T_{max}, and sulfur content. The S1 (mgHC/gRock) indicates the volume of free hydrocarbons present without thermal cracking of the kerogen at

Table 2
RockEval parameters of the selected samples from Jordanian oil shale.

Sample Name	T_{max} (°C)	HI	OI	PI	S1 (mg/g)	S2 (mg/g)	S3 (mg/g)	Total Sulfur (%)	TOC (%)
Jordan-1	420	822	8	0.03	4.96	147.52	1.35	3.68	17.94
Jordan-2	419	847	9	0.03	4.17	136.69	1.5	2.94	16.15
Jordan-3	420	858	8	0.03	4.01	127.78	1.22	3.09	14.89
Jordan-4	418	861	9	0.04	4.41	111.37	1.14	3.06	12.93

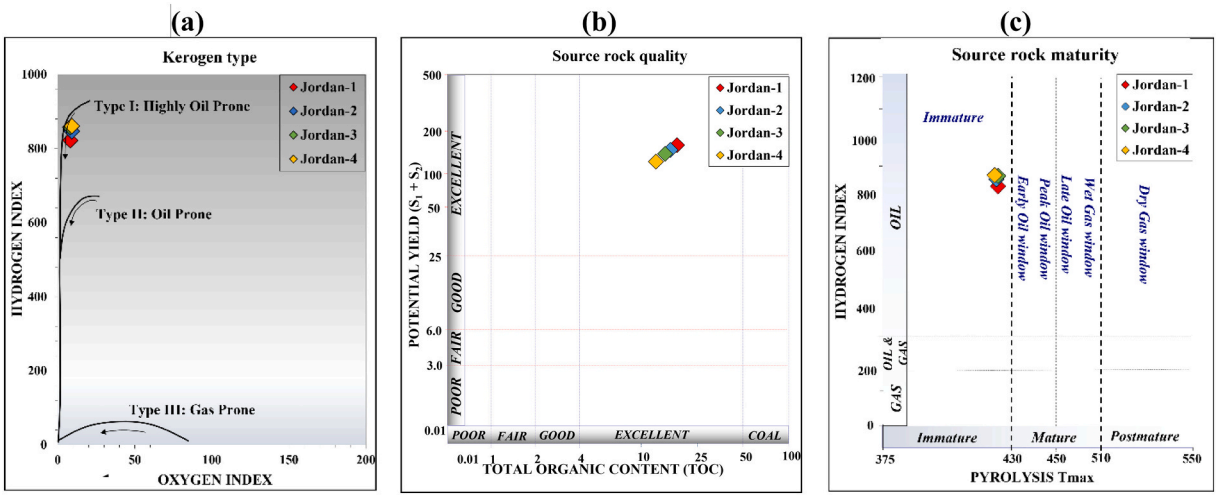

Fig. 3. Analyzed Jordanian oil shale rock parameters derived from RockEval pyrolysis: a) kerogen type, b) source rock quality, and c) source rock maturity.

Table 3
Mineralogy from x-ray powder diffraction (XRD) analysis and total organic carbon.

Sample No.	Mineral composition from XRD		
	Mineral phase	Chemical formula	Abundance %
Jordan-1	Calcite	$CaCO_3$	85
	Quartz	SiO_2	14
	Berlinite	$Al(PO_4)$	1
Jordan-2	Calcite	$CaCO_3$	92
	Quartz	SiO_2	4
	Apatite	$Ca_5[PO_4]_3(OH,F,Cl)$	4
Jordan-3	Calcite	$CaCO_3$	73
	Quartz	SiO_2	14
	Apatite	$Ca_5[PO_4]_3(OH,F,Cl)$	12
	Langite	$Cu_4(SO_4)(OH)_6{\cdot}2H_2O$	1
Jordan-4	Calcite	$CaCO_3$	44
	Quartz	SiO_2	54
	Apatite	$Ca_5[PO_4]_3(OH,F,Cl)$	1.4
	Berlinite	$Al(PO_4)$	0.5

approximately 300 °C. In addition, S2 (mgHC/gRock) is the quantity of hydrocarbons produced due to thermal cracking from 300 °C to 600 °C, whereas S3 ($mgCO_2$/gRock) indicates the amount of CO_2 produced during the programmed pyrolysis. Finally, T_{max} (°C) is the temperature for the maximum peak of S2 and denotes the source sample maturity. Sulfur content is measured during pyrolysis and oxidation with temperatures up to 1200 °C.

The TOC percentage of the rock is determined by the oxidation in the air in a second oven from the residual organic carbon after pyrolysis. Other functional parameters are also calculated from the parameters, including the oxygen index (OI = S3/TOC), hydrogen index (HI = S2/TOC), production index (PI = S1/(S1 + S2)), and hydrocarbon potential (S1 + S2). All results are checked and calibrated using the Institut Français du Pétrole Energies Nouvelles standards.

The Jordan source rock samples displayed varying TOC ranging from 13 % to 18 %. The parameters from RockEval 7S are presented in Table 2. The samples are numbered descending from the highest (Jordan-1) to the lowest (Jordan-4) TOC, whereas the HI indicates a slight increase with the decrease in TOC. A modified Van Krevelen diagram is plotted against the HI and OI of the analyzed samples, suggesting a Type II kerogen with high sulfur content (Fig. 3(a)). This type of kerogen represents the deposition of organic matter in marine environments under euxinic conditions. A cross-plot between the TOC and hydrocarbon potential yield (S1 + S2) characterized the studied source rocks samples as having excellent quality (Fig. 3(b)). However, the corresponding T_{max} values for these samples are low (about an average of 419 °C). The low T_{max} values suggest that the studied source rock has not reached the optimum thermal maturity window to generate hydrocarbons and is therefore characterized as an immature source rock interval (Fig. 3(c)). The complex pyrolysis plots for each sample are displayed in the appendix (Figs. A.2 to A.4).

2.3. Bulk mineralogy determination of Jordanian oil shale samples

The mineralogical composition of the tested Jordanian oil shale samples was determined through an x-ray powder diffraction (XRD) analysis (RAYONS x-ray instrument) [81]. The equipment applied a cobalt Kα radiation source at 40 mA and 40 kV. A Rietveld x-ray diffractometer was used for achieving the XRD patterns and Rietveld refinement. High Score Plus software was used to identify the size of each phase.

The mineralogy presented in Table 3 indicated that a significant composition of the samples is calcite and quartz with very few traces of phosphate minerals (i.e., berlinite and apatite). Nevertheless, some variation exists in the mineral abundance between the analyzed samples, as illustrated in Table 3. The highest calcite abundance was found in Jordan-2 at 92 wt%, and the lowest was in Jordan-4 at 44 wt%. Jordan-1 and 3 demonstrated a high calcite abundance of 85 % and 73 %, respectively. While Jordan-1, 2, and 3 have a low quantity of quartz (between 4 and 14 wt%), Jordan-4 contains 54 wt%. Overall, the XRD findings suggest that the samples contain minerals ordinarily present in shale rocks.

2.4. Surface characterization and pore-size determination of Jordanian oil shale samples

Scanning electron microscopy (SEM) was conducted using the Quattro SEM instrument. The SEM images in Fig. 4 demonstrated that the samples were fine-grained and moderately to poorly sorted, ranging from packstone (Jordan-1, 2, and 3) to wackestone (Jordan-4). The images display inter-particle porosities with small moldic porosities filled with bio-micritized clasts of peloids, plankton foraminifers, bryozoans, and echinoderms that indicate the heterogeneity of the packed shale source rock.

A Tristar II (3020) instrument was used to conduct low-pressure nitrogen (N_2, 99.999 vol%) adsorption-desorption isotherm measurements at 77 K to measure the pore volume, specific Brunauer–Emmett–Teller (BET) surface area, and average pore size of the rocks. The pore system among all samples is primarily reduced by syntaxial calcite cement and the bio-micrite volume. The packing influence

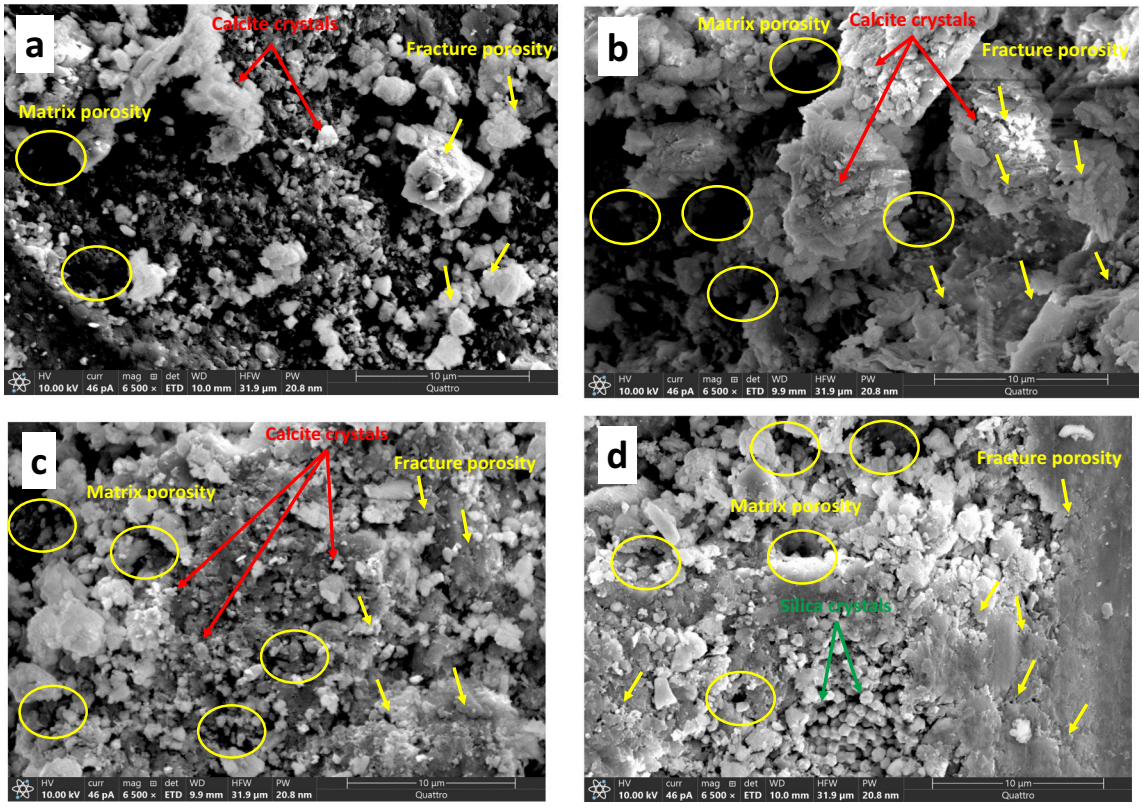

Fig. 4. Scanning electron micrographs of Jordanian oil shale samples: a) Jordan-1, b) Jordan-2, c) Jordan-3, and d) Jordan-4.

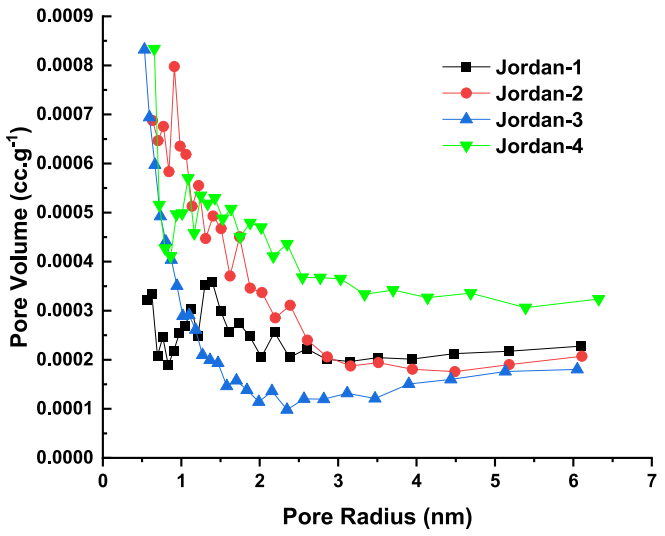

Fig. 5. Associated pore-size distribution of the analyzed Jordanian oil shale samples.

Table 4
Textural properties of the examined samples (summary of N_2 Brunauer–Emmett–Teller (BET) surface area).

Sample Name	Jordan-1	Jordan-2	Jordan-3	Jordan-4
Specific surface area, m^2/g	3.08	3.68	3.53	3.19
Pore volume, cm^3/g	0.032	0.031	0.024	0.011
Average pore throat radius, nm	20.7	17.3	13.62	7.365
Type of pores (2–50 nm)	Mesopores	Mesopores	Mesopores	Mesopores

of various calcified components on the pore system presented by the SEM images (Fig. 4) is reflected in the pore distribution from the N_2 adsorption/desorption isotherms in Fig. 5.

The average pore-size distribution measured from the N_2 adsorption-desorption isotherms of all analyzed samples ranges from 15 to 42 nm (Table 4), indicating a mesoporous system (below 50 nm) with a negligible presence of micropores according to IUPAC nomenclature (Rouquerol et al., 1994). Furthermore, the total volume was measured at relatively low pressures approaching 1, based on the N_2 adsorption-desorption isotherms (Table 4).

2.5. *Surface functional groups and topography of Jordanian oil shale samples*

The chemical active functional groups on the surface of the rock were characterized (within a wavenumber of 650–4000 cm^{-1}) through Fourier transform infrared (FTIR) spectroscopy analysis using a PerkinElmer spectrometer (100-FTIR instrument). The FTIR spectra of the Jordanian shale samples are presented in Fig. 6, which demonstrates a series of peak patterns with diversified functional groups (Table 5). The spectra primarily characterize band series of vibrations of calcium carbonate (CO_3^{-2}) ions at the band from 690 to 874 cm^{-1} and at peaks of 2853 and 2927 cm^{-1} (Andersen and Brečević, 1991; Rodriguez-Blanco et al., 2011).

The highest sharp stretching characteristics of hydrocarbons were demonstrated at 1420 cm^{-1}, which most likely represents C—H bonding and refers to the presence of hydrocarbon film on the surface of the rock samples. Additionally, other peaks of H functional groups might be observed at 2853 and 2927 cm^{-1}. There is a broad mountain centered at about 3622 and 3699 cm^{-1}, a characteristic of the hydroxyl O—H stretching mode of alcohols. The breadth of this signal is a consequence of H_2 bonding between molecules. Furthermore, bands of free-electron functional groups are recognized: a weak carbonyl peak $C=\ddot{O}$ at

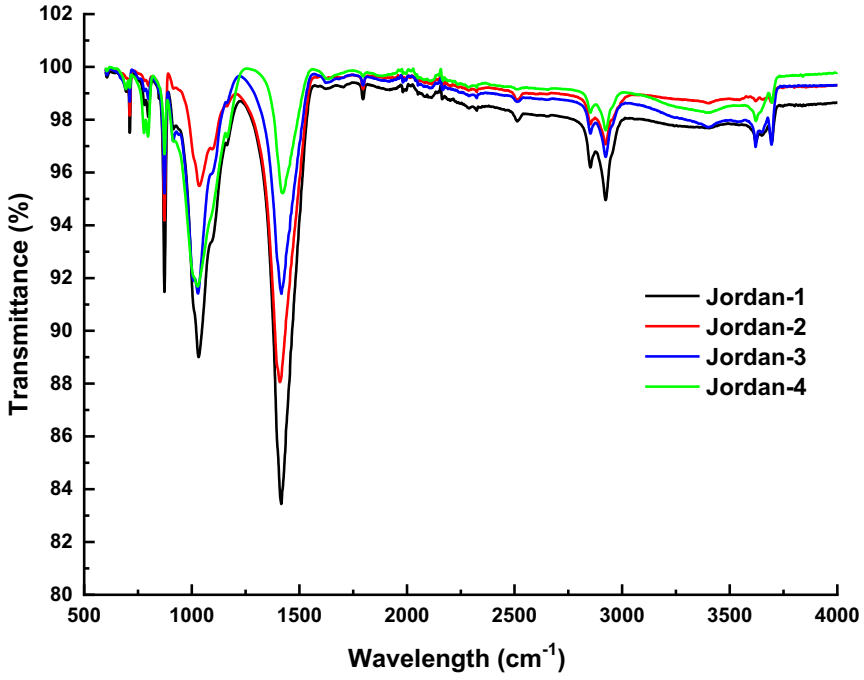

Fig. 6. Fourier transform infrared spectra of Jordanian oil shale samples at different depths.

Table 5
Fourier transform infrared spectra signals in Jordanian shale source rock samples based on guidelines provided by Coates (2006).

Peak wave number [cm^{-1}]	Proposed assignment	Mineral/compound	Reference
778–875	In-plane bending mode of CO_3^{-2}	Calcite or vaterite	Rodriguez-Blanco et al. [82]; Andersen and Brecevic [83]
695–712		Calcite	Kiefer et al. [84]; Ji et al. [85]; Chakrabarty and Mahapatra [86]
871	Out-of-plane bending vibration of CO_3^{-2}	Calcite	Kiefer et al. [54]; Wang et al. [87]
1030	S=O stretching	In sulfoxide	Coates [88]
1083	Symmetric CO_3^{-2} stretching vibration		Wang et al. [87]
1420	C-H stretching vibrations	Hydrocarbon film	Nandiyanto et al. [89]
1626	C=C in stretching	In alkene	Nandiyanto et al. [89]
1798	COOH functional group in aromatic compounds	Combination of a broad –OH stretch and a C=O stretching peak in ester (arachidyl dodecanoate)	George et al. [90]
2853	In-plane bending mode of CO_3^{-2} and CH groups	In alkane compounds	Ji et al. [85]
2927	In-plane bending mode of CO_3^{-2} and CH groups	In alkane compounds	Ji et al. [85]
3622	Primary O—H group	In organic compounds	Coates [88]
3699	Secondary O—H group	In organic compounds	Coates [88]

Table 6
Root mean square surface roughness obtained from atomic force microscopy.

Surface roughness (nm)			
Jordan-1	Jordan-2	Jordan-3	Jordan-4
136	89	142	399

1798 cm^{-1} and a middle peak of sulfonyl groups $S=\ddot{O}$ at 1030 cm^{-1}.

The distribution of the peaks varies among the analyzed samples. The carbonate ion (CO_3^{-2}) signals descend from the highest peak in Jordan-1, followed by Jordan-2 and 3, to the lowest in Jordan-4. Similarly, the C—H bond stretching at 1420 and 2853 cm^{-1} and bond bending at 2927 cm^{-1} follow the same trend, corresponding to the variation in TOC from the highest (Jordan-1) to the lowest (Jordan-4). In addition, the carboxyl group (COOH) stretching vibrations observed at 1798 cm^{-1} demonstrated a similar signal trend between samples. Only the stretching frequencies of sulfonyl functional groups at 1030 cm^{-1} and the hydroxyl functional groups at 3622 and 3699 cm^{-1} displayed some variation. The $S=\ddot{O}$ bond is more firmly in Jordan-1 (the highest TOC) than Jordan-4, where Jordan-1 > Jordan-4 > Jordan-3 > Jordan-2. While the peaks of the O–H bond stretching were observed as follows: Jordan-3 > Jordan-1 > Jordan-4 > Jordan-2. A detailed explanation of the major signals in the FTIR spectrum of the source rock samples is presented in Table 5.

The surface roughness of the Jordanian oil shale samples was determined using atomic force microscopy (AFM; Flex-Axiom, Nanosurf with a C3000i controller). The AFM results of the studied samples are presented in Table 6 and Fig. 7. The order of increasing surface roughness based on the AFM results is Jordan-4 > Jordan-3> Jordan-1 > Jordan-2. Previous studies have revealed that the contact angles of CO_2/brine and H_2/brine systems on storage rocks decreased with increasing surface roughness and that the brine advancing/receding angles measured on smooth surfaces are higher than those on rough surfaces because the brine droplet diffuses quickly into the grooves on uneven surfaces [91–93]. However, the variations in surface roughness among the Jordanian oil shale samples used for this study should have no significant effect on the contact angle values because the changes in surface roughness between each sample were <1 μm (1000 nm) [93].

a) Jordan-1

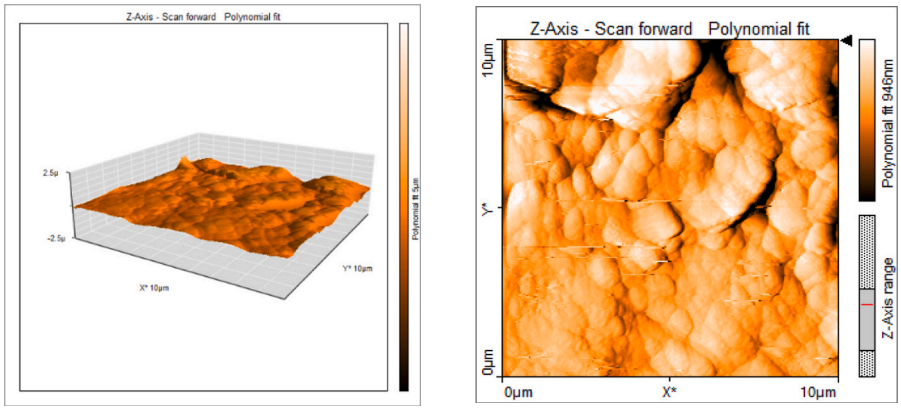

b) Jordan-2

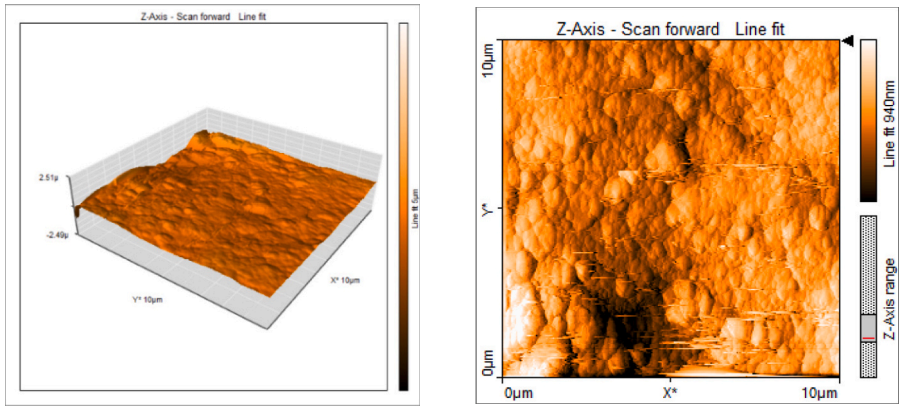

c) Jordan-3

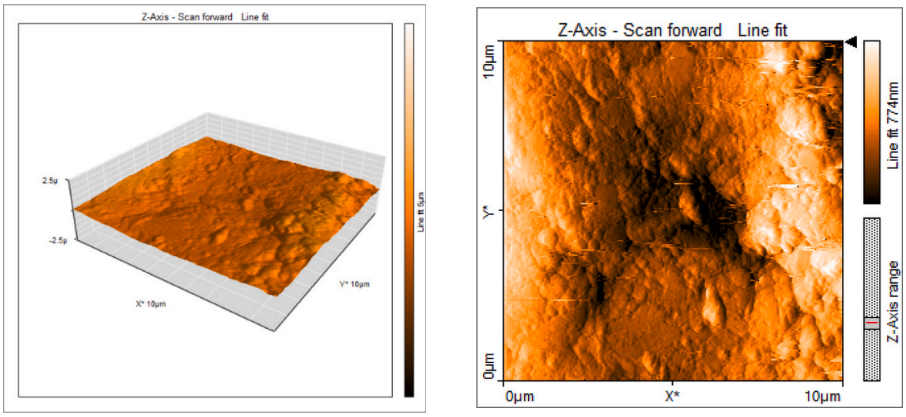

d) Jordan-4

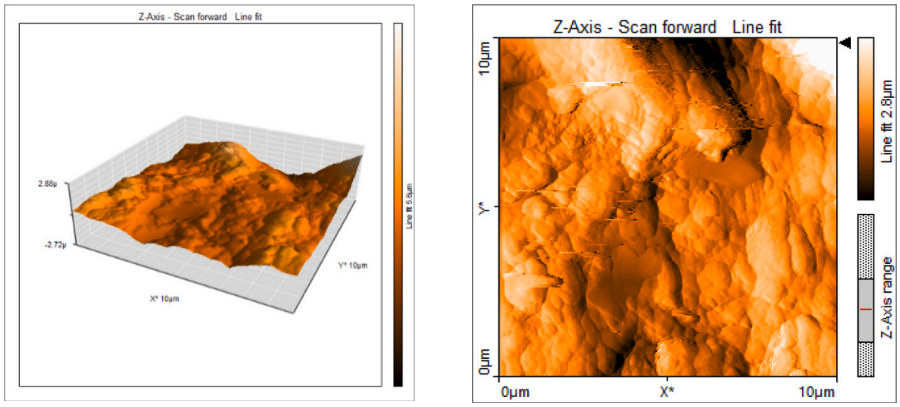

Fig. 7. Two- and three-dimensional topography of the four Jordanian source rock samples.

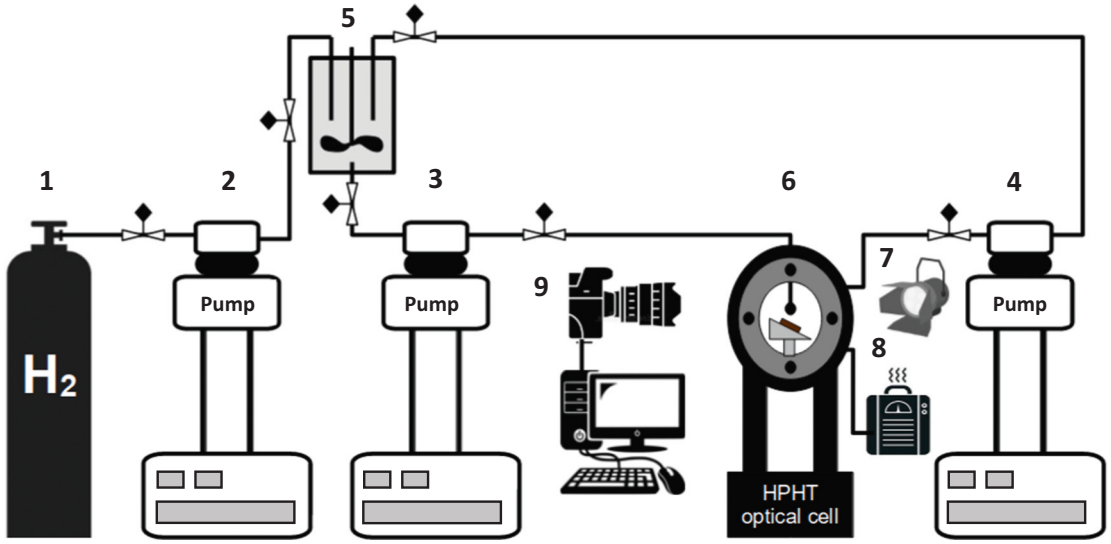

Fig. 8. Schematic of high-pressure, high-temperature (HPHT) contact angle system: (1) Gas bottle, (2) ISCO syringe pump for gas, (3) HPHT Hastelloy cell with tilted plate housing, front view, (4) ISCO syringe pump for live brine, (5) brine feed source, and (6) high-resolution video camera with acquisition and interpretation system.

2.6. Interfacial tension and contact angle measurement

Contact angles (advancing and receding) were measured in high-pressure, high-temperature (HPHT) cells using the tilted plate technique (17°) to assess the wetting behaviors of organic-rich carbonate rock in the presence of H_2/brine, CH_4/brine, and H_2-CH_4/brine mixture systems [94]. Two Teledyne ISCO D-260 pumps were connected to the HPHT cell to introduce fluids into the viewing cell (the pressure precision is 0.01 %). Thermodynamic equilibration was conducted in a mixing reactor (500 mL Parr) affixed to the gas cylinder (H_2 and CH_4) and the brine ISCO pump to prevent mass transfer effects between the gases (H_2 and CH_4) and brine during contact angle experiments. The Jordanian sample thin section was positioned in the IFT cell, followed by gas injection (H_2, CH_4, or H_2-CH_4 mixture). The fluid temperature in the viewing cell and ISCO pumps was maintained using a heating tape and controller (HTC101–002) and a heating bath (900 °F, Julabo), respectively. Once the experimental pressure and temperature conditions were reached, a droplet (5 ± 0.75 μL drop size) of equilibrated brine (1 % KCl + 2 % NaCl) was dispersed. Initially, the IFT measurements were conducted at the point where the droplet was about to leave the needle; afterward, it was dispensed onto the rock surface. The contact angles were recorded at the droplet's leading (for advancing contact angles) and trailing edges (for receding contact angles). A high-performance camera was used to video-record the procedure, and contact angles were measured with ImageJ software for further analysis. We repeated the experiments thrice and computed the average standard deviation (±3) based on repeated measurements. A schematic of the experimental setup for the contact angles and IFT measurements is presented in Fig. 8.

3. Results and discussion

Rock-fluid interaction and wetting characteristics are crucial parameters controlling gas spread through a geological formation [95–97]. They regulate the storage capacity [62,98,99], fluid dynamics, and flow throughout the porous media [98,100,101]. In addition, they control the gas injection rates [100,102], gas withdrawal rates [29,103–105], and gas entrapment safety [106–109]. In this context, the receding contact angle is for the condition where gas is injected and brine is displaced. When θ_r is >90°, it may affect the structural entrapment of gas [110]. Further, the advancing contact angle describes the situation in which brine imbibes again and entraps the gas in clusters, causing residual trapping. When θ_a is >50°, it may affect the primary drainage [104,111–113]. Natural geo-storage formations have an inherent organic presence, which may significantly affect the storage capacity [114–116]. Therefore, contact angles (θ_a and θ_r) were measured for four Jordanian oil shale samples with various TOC at various pressures and temperatures (0.1–1600 psi and 323 K) and compared further with other shale TOC geological formations. Moreover, IFT measurements were conducted for H_2/brine, CH_4/brine, and H_2-CH_4/brine mixtures at similar HPHT conditions, which can further be used for gas column height calculations.

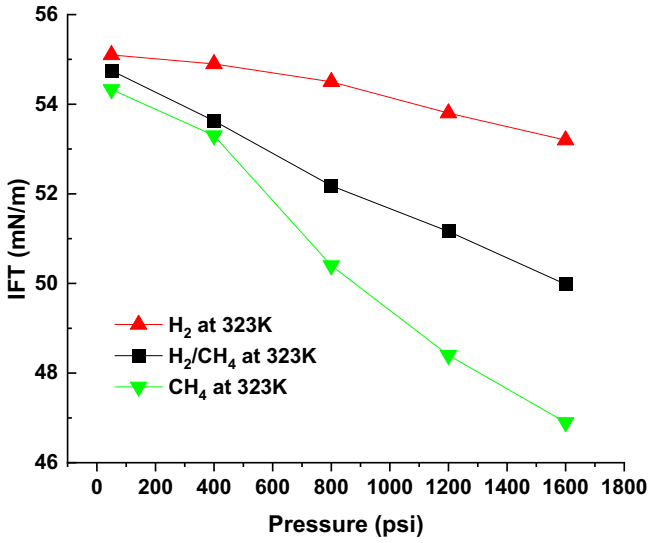

Fig. 9. Measured interfacial tension (IFT) between gas and liquid (10 wt% NaCl brine) for H_2/brine, CH_4/brine, and H_2-CH_4/brine mixture (50 %/50 %) systems at varying pressures (50–1600 psi) and 323 K using a high-pressure high-temperature contact angle IFT system. The uncertainty based on repetitiveness is from ±1.7 to ±2.3 mN/m.

3.1. Interfacial tension of H_2/brine, CH_4/brine, and H_2-CH_4/brine

The measured IFT values for H_2/brine, CH_4/brine, and H_2-CH_4/brine

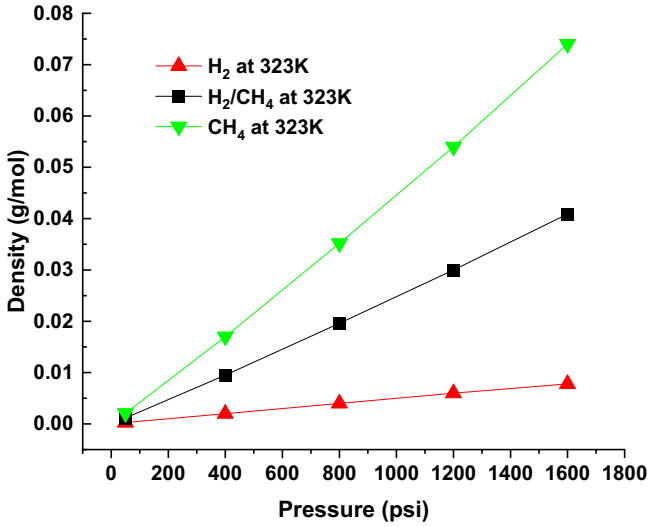

Fig. 10. Density of H_2/brine, CH_4/brine, and H_2-CH_4/brine mixture (50 %/50 %) systems at varying pressures (50–1600 psi) and 323 K [126].

systems are presented in Fig. 9. The IFT generally decreased with increasing pressure. However, the change in the CH_4/brine IFT with increasing pressure was more significant than that of the H_2/brine IFT. The steep drop beyond around 400 psi of the CH_4/brine IFT is attributed to reaching critical CH_4 conditions (i.e., 673 psi and 190.55 K). Moreover, the highest IFT values were measured in pure H_2, whereas the pure CH_4/brine IFT values were the lowest. For instance, at 323 K, the IFT value of pure H_2/brine slightly decreased from 55 to 53 mN/m, whereas the CH_4/brine IFT values decreased from 54.5 to 46.5 mN/m with increasing pressure from 200 to 1600 psi. As expected, the IFT values of H_2-CH_4/brine range between pure H_2 and pure CH_4. This trend agrees with IFT data previously reported for gas/brine IFT as a function of pressure in previous research. The trend can be attributed to increasing intermolecular cohesive interaction and decreasing the adhesive force between the brine and gas molecules due to rising gas densities with increasing pressure [6,18,36,117].

Similarly, the lower pure CH_4/brine IFT and H_2-CH_4/brine IFT compared to pure H_2/brine IFT can be attributed to higher densities of pure CH_4 and the CH_4-H_2 mixture compared to pure H_2 (Fig. 10), resulting in better interaction of pure CH_4 and CH_4-H_2 molecules at the interface in comparison to the H_2/brine system. Previous studies have also demonstrated that H_2 molecules have higher bond strength (cohesive action) and a lower relative brine solubility than CH_4 molecules [33,43].

Thus, it is likely that more pure CH_4 and H_2-CH_4 mixture molecules accumulated at the interface (due to their higher density) compared to pure H_2, which increased interfacial activity for CH_4/brine and H_2-CH_4/brine compared to pure H_2/brine systems. During UHS, the containment security of H_2 and the storage potential of the storage rocks (capillary/residual trapping capacities) and sealing integrity of the caprock (structural trapping capacities) are significantly influenced by the capillary pressure (P_c) presented in Eq. (1) [118,119]:

$$P_c = P_{H_2} - P_{water} = \frac{2\gamma cos\,(\theta)}{r}, \quad (1)$$

where the H_2/brine IFT (γ) is in mN/m, and r is the capillary radius (average pore size of the rock) in nanometers (nm). The upward movement of the buoyant H_2 and leakages of the stored H_2 across the caprock are promoted when the capillary force is lower than the buoyancy pressure or buoyancy force of the H_2 plume [98,99,120]. The possibility of H_2 leakage across the caprock is high when the threshold capillary pressure is exceeded [23,53,121,122]. Lower contact angle values and higher H_2-brine IFT values are necessary for maintaining

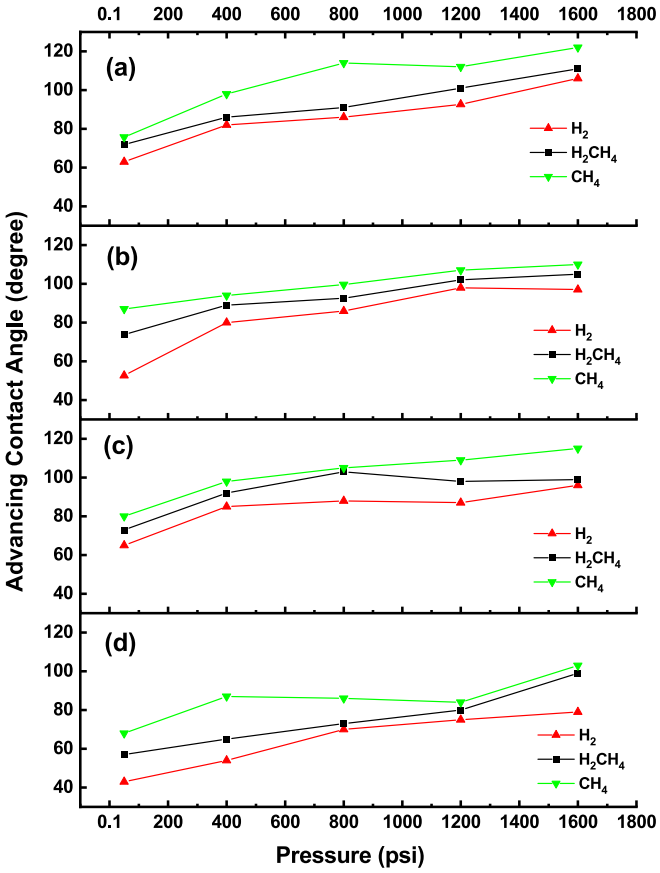

Fig. 11. Advancing contact angles of H_2/brine, CH_4/brine, and H_2-CH_4/brine mixture (50 %/50 %) systems on Jordanian oil shale samples at 323 K: a) Jordan-1, b) Jordan-2, c) Jordan-3, and d) Jordan-4. The average uncertainty obtained from repetitive measurement is ±3°.

higher capillary pressure (high residual and structural trapping potential) [5,123–125].

We observed that the mixture of a potential cushion gas during UHS (CH_4) along with H_2 resulted in decreasing the IFT compared to the pure H_2/brine IFT, suggesting that the risk of stored H_2 diffusion across the caprock is high at the mixing zone between the stored gas and cushion gas (H_2-CH_4 mixture). Thus, we infer that the structural trapping of H_2 by the caprock reduces due to the H_2-CH_4 mixing zone and anticipated lower breakthrough pressure from decreasing the IFT. However, all studied Jordanian oil shale samples are high TOC shale and can only serve as the storage for H_2 through adsorption trapping mechanisms. The TOC values of the Jordanian oil shale samples as measured through RockEval pyrolysis are 13 %, 15 %, 16 %, and 18 %, corresponding for Jordan-4 to 1 in this study, arranged respectively based on the TOC. For such rocks, the increasing hydrophobicity of organic-rich rock promotes the adsorption trapping of H_2 in kerogen and the subsequent production (expulsion) of CH_4 from organic-rich rocks.

3.2. Pressure and gas mixing effect on H_2/brine, CH_4/brine, and H_2-CH_4/brine wettability

Previous research has addressed the influences of wetting behaviors on storage formation and caprock for the success of UHS in sandstone and carbonate formations [29,53,55,121,127]. However, the influence of H_2-cushion gas mixed-zone wettability on the containment security of H_2 in organic-rich shale source rocks has never been reported in the literature, to the best of the authors' knowledge. We measured contact angles at 323 K and varying pressures (0.1–1600 psi) to assess the effect of pressure and gas type (pure CH_4, pure H_2, and H_2-CH_4 mixtures) on

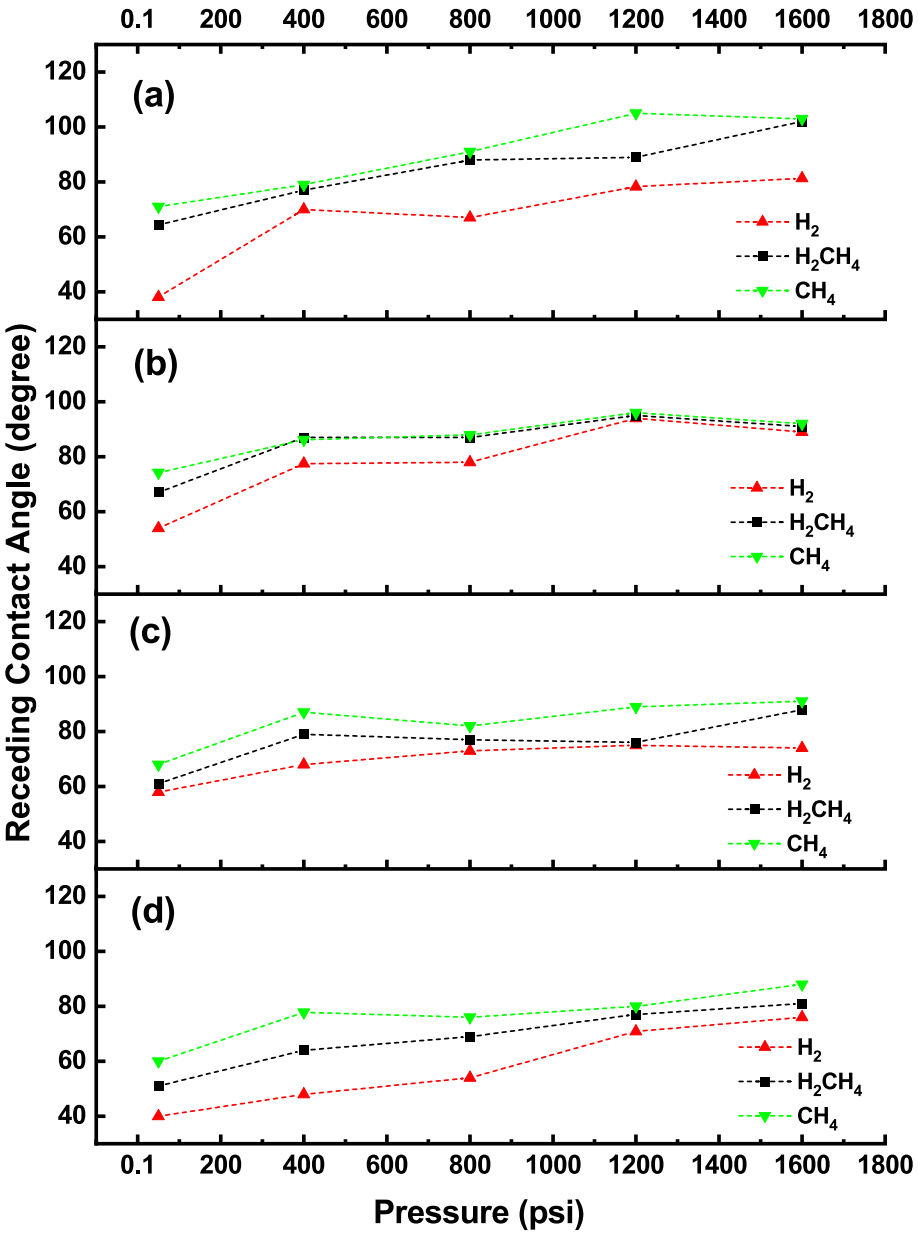

Fig. 12. Receding contact angles of H_2/brine, CH_4/brine, and H_2-CH_4/brine mixture (50 %/50 %) systems on Jordanian oil shale samples at 323 K: a) Jordan-1, b) Jordan-2, c) Jordan-3, and d) Jordan-4. The average uncertainty from repetitive measurement is ±3°.

the wettability of organic-rich shale source rock.

The contact angles of H_2, CH_4, and H_2-CH_4 mixtures on organic-rich shale rocks at various pressures are presented in Figs. 11 and 12 and Table A.1. The plotted contact angle datasets indicate that the gas type demonstrated varying characteristics on the studied Jordanian oil shale samples (Jordan-1 to 4) at various pressures. The contact angles generally increased with increasing pressure due to the increasing gas densities and intermolecular cohesive forces at higher pressures, promoting the interaction between the gas molecules and rock surfaces at higher pressures [30,128,129].

For instance, considering the Jordan-4 sample with the lowest TOC (13 wt%), the contact angles of H_2/brine systems ranges between 43° and 79° (for θ_a) and 43° and 76° (for θ_r), suggesting a weakly water-wet condition as the pressure ranges between 50 and 1600 psi at 323 K. At the same pressure range and temperature conditions, the contact angles of CH_4/brine systems range between 68° and 103° (for θ_a) and 60° and 88° (for θ_r), indicating weakly water-wet to intermediate-wet conditions. Similarly, at similar pressure ranges and temperature conditions, the contact angles of H_2-CH_4/brine systems range between 73° and 99° (for θ_a) and 61° and 88° (for θ_r), suggesting weakly water-wet to intermediate-wet conditions (Figs. 11 and 12).

These results can be attributed to the density differences between H_2, CH_4, and the H_2-CH_4 mixture, as depicted in Fig. 10. The interactions between the CH_4 molecules and the surface of the rock are higher than those for H_2 molecules and the rock surface. The results indicate that the contact angles of CH_4 are higher than those of the H_2 contact angle (CH_4 > H_2-CH_4 > H_2). This outcome implies that the rock is less water-wet at the H_2-CH_4 mixing zone than in the working zone. The increasing predisposition of the rock to become more hydrophobic at the H_2-CH_4 mixing zone is beneficial for the adsorption trapping mechanism, which favors the adsorption of gas molecules in micropores [60,65]. This predisposition permits significant quantities of H_2 to be trapped on kerogen and the subsequent CH_4 expulsion (recovery) from the organic-rich Jordan shale formation [33,43].

In contrast, higher contact angles of H_2-CH_4 mixtures on the Jordanian oil shale samples than those of pure H_2 also suggest that capillary

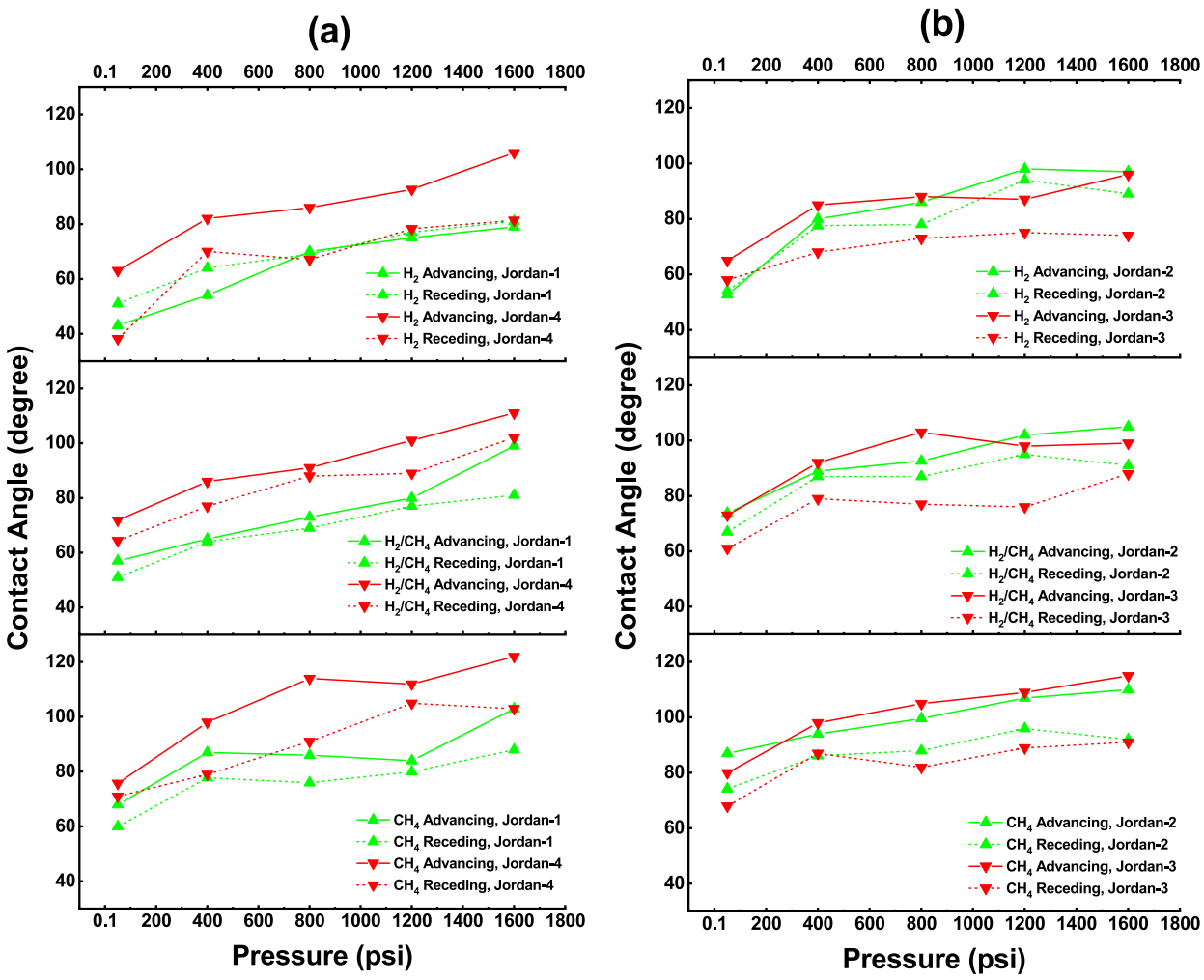

Fig. 13. Advancing and receding contact angles of H_2/brine, CH_4/brine, and H_2-CH_4/brine mixture (50 %/50 %) systems as a function of pressure and total organic carbon (TOC) at 323 K – a) highest TOC (Jordan-1, TOC = 18 %) and lowest TOC (Jordan-4, TOC = 13 %) and b) intermediate TOC samples (Jordan-2, TOC = 16 %; Jordan-3, TOC = 15 %).

entry pressure is lower and that the associated structural integrity of caprock for H_2 entrapment is lower [98,102,130]. Generally, as the receding contact angles increase beyond 90°, an upwardly directed suction force (lower capillary pressure) initiates that significantly increases the capillary leakage (risk of H_2 leakage via the caprock), reduces H_2 column heights, and reduces containment security.

3.3. *Effect of total organic carbon on H_2/brine, CH_4/brine, and H_2-CH_4/brine wettability*

Organic acids are inherently available in formation water due to reductive conditions where anoxic situations thrive [3,114–116]. The presence and quantity of organic materials depend on the formation type. However, a minimal existence is enough to significantly influence the petro-physical (i.e., pore system), petro-graphical (i.e., mineralogy and elemental composition), and wetting characteristics of any geological formation [131–133], affecting gas entrapment safety and storage quantity [6,117]. Moreover, the organic-rich shale formations have an abundance of organics (straight and branched chain), similar to the studied Jordanian oil shale rocks [61,62,134,135]. Recently, some studies have demonstrated the functional dependence of gas wettability on organics, source rock type, and TOC [62,136–138].

In this section, the influence of TOC on H_2/brine, CH_4/brine, and H_2-CH_4/brine systems for the four Jordanian oil shale samples was investigated for a wide range of pressures (0.1–1600 psi) at 323 K. The dynamic contact angles for the analyzed samples are illustrated in Fig. 13, indicating an increasing trend with TOC ranging from 13 to 18 wt% (high to ultrahigh) for all three gas systems. The results imply a shift in wettability status from intermediate-wet ($70° < \theta < 110°$) to weakly H_2-wet ($110° < \theta < 130°$) [99,139]. For example, the advancing contact angle for the H_2/brine system for Jordan-1 at 1600 psi and 323 K increased from 96° to 106°, whereas for CH_4/brine and H_2-CH_4/brine systems, it increased from 115° to 122° and 99° to 111°, respectively. Additionally, the receding contact angle at the same conditions rose from 76° to 81°, 88° to 103°, and 81° to 102° for H_2/brine, CH_4/brine, and H_2-CH_4/brine systems, respectively.

Comparing the highest (Jordan-1) and lowest TOC (Jordan-4), Fig. 13(a) indicated that the contact angle increase is also a function of pressure. As the pressure increased, the higher TOC sample exhibited higher contact angles, and the lowest TOC sample displayed the lowest contact angles. This outcome indicates a higher shift toward H_2-wet conditions for higher TOC samples. Jordan-2 and 3 displayed close behavior regarding the difference in TOC for both samples at only 1 wt %. Hence, no significant discrepancy was identified in Fig. 13(b) because both samples have similar mineral compositions, as presented in Table 3, particularly in calcite and quartz content.

The average increments in contact angles due to the increase in TOC from 13 to 18 wt% are approximately 10° in advancing and 15° in receding angles, implying that TOC has a more pronounced influence on the receding contact angle. In the context of H_2 geo-storage, the receding

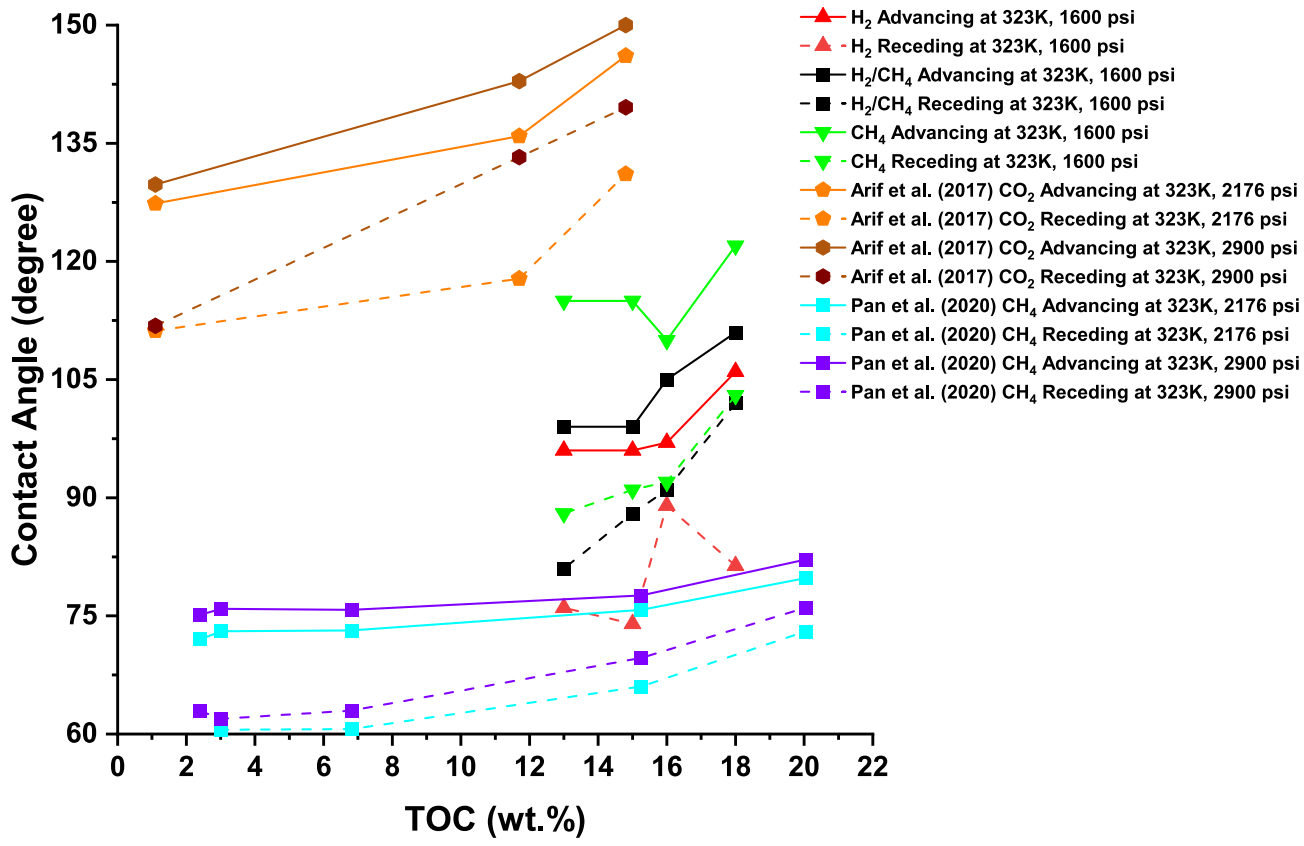

Fig. 14. Advancing and receding contact angles of H_2/brine, CH_4/brine, and H_2-CH_4/brine mixture (50 %/50 %) systems as a function of total organic content (TOC) for Jordanian oil shale samples, including CO_2/brine contact angles of high TOC shale from Arif et al. (2017) [62] and CH_4/brine from Pan et al. (2020) [61]. The average uncertainty from repetitive measurement is ±3°.

contact angle typically represents the structural trapping mechanism, a significant H_2 trapping mechanism in geological formations [39,121,140]. Moreover, the effect of TOC is consistent with previous studies (Fig. 14) [61,62].

The function of shale TOC for CO_2/brine and CH_4/brine systems has behaved similarly in previously reported studies for wettability measurements at various geo-storage conditions in terms of pressure and temperature [61,62]. The brine contact angles increased for CO_2 and CH_4 gases as TOC increased. The current study reported a similar increase, which implies that inherent organic materials in shale formations have a strong affinity with the rock matrix, making it hydrophobic [3,61]. However, CO_2/brine contact angles were higher than other gases and mixtures at all tested HPHT conditions due to the difference in gas densities and intermolecular attraction of gas molecules to the rock surface [128]. Comparative studies have provided a wide range of shale TOC from 0.1 to 20 wt% compared to this study (13 to 18 wt%). Although the current study does not focus on varying temperature, one major similarity between the study by Pan et al. (2020) [61] and this study is the CH_4/brine contact angles. The brine contact angles reported in this study for CH_4 gas are higher than those reported for CH_4 by Pan et al. [61] due to the difference in the formation type and salinity (5 wt% NaCl for Pan et al. [61] and 2 wt% NaCl +1 wt% KCl for this study). Organics profoundly influence the wetting characteristics and associated storage capacities compared to other influencing parameters. Therefore, it is pertinent to gauge the effect of organics in simulation studies for correct estimations, and ramifications should be considered before the injection of gases for geo-storage purposes.

This research evaluated a natural organic-rich shale source rock, which is a promising candidate for H_2 storage and inherently contains organic acids, to assess the influence of organic materials on the wettability of H_2-CH_4/brine/rock systems and the H_2-CH_4/brine IFT. The study further evaluated the suitability of CH_4 as a cushion gas for UHS and highlighted the contributions of organic contamination to the H_2 containment security of natural organic-rich shale source rocks. However, the H_2-CH_4/brine reactions with the host rocks, which also significantly affect the storage potential of the source rock, were not studied.

4. Conclusions

Underground storage of H_2 in geological formations has been suggested as an effective technique of ensuring energy security by storing a large volume of H_2 in geo-storage formations until critical energy demand is reached [11,16–19,24,36,141–143]. Before H_2 injection into the subsurface, cushion gas injection is required to maintain the pressure in the formation and enable facile retrieval of the stored H_2 when needed [42,72,144]. Thus, a working gas zone (H_2, in this case), mixing zone (H_2-CH_4, in this case), and cushion gas zone (CH_4, in this case) must exist at the geo-storage formations [17,39,42]. There is a lack of information on the wetting characteristics and gas/brine IFT for organic-rich rock samples. This research was conducted to provide insight into the rock-wetting behaviors and gas/brine IFT during UHS in Jordanian oil shale samples. The following conclusions were reached.

1. Advancing contact angles of H_2-CH_4/brine systems on four studied samples ranged between 57° and 111°, whereas the receding contact angles ranged between 51° and 102° when pressure increased from 50 to 1600 psi at 323 K. This result indicates that the organic-rich shale source rocks demonstrated weakly water-wet to weakly H_2-wet conditions at the mixing zone.
2. The pure CH_4/brine system demonstrated a higher rock-wetting tendency (higher contact angles) and the lowest gas/brine IFT

compared to H_2/brine systems under all studied pressure and temperature conditions, suggesting a higher interaction between the CH_4 molecules and rock compared to H_2. Thus, CH_4 may be used as a favorable cushion gas during H_2 storage to maintain the formation pressure.

3. The effects of pressure and temperature on the wettability and IFT of pure H_2/brine, pure CH_4/brine, and H_2-CH_4/brine systems displayed similar behavior, where higher contact angles and lower gas/brine IFT were measured at higher pressures, which is consistent with the literature [61,62].
4. When cushion gas is injected into a geo-storage formation before H_2, the H_2-CH_4 mixture could result in decreased capillary pressure (due to reducing the IFT and increasing the contact angles), suggesting that the risk of stored H_2 diffusion across the caprock could be high at the mixing zone between the stored gas and cushion gas (H_2-CH_4 mixture). However, the increasing rock hydrophobicity could increase the adsorbed H_2 molecules on rock micropores. Thus, more H_2 could be trapped on the kerogen of rock through adsorption trapping, resulting in CH_4 production and a balance between enhanced CH_4 recovery and reduced/decreased capillary trap/structural entrapment.
5. Although higher contact angles and lower IFT for the H_2-CH_4/brine system suggest that the trapping capacity of H_2 could be reduced at the H_2-CH_4 mixing zone due to the anticipated lower breakthrough pressure, the increasing affinity of these rocks to the CH_4 instead of H_2 could decrease the likelihood of H_2 diffusion into the pore space, promoting easier separation during H_2 injection and withdrawal cycles.
6. The influence of TOC on H_2/brine, CH_4/brine, and H_2-CH_4/brine systems was also investigated for a wide range of pressures (0.1–1600 psi) at 323 K. The results indicated a significant shift in wettability from intermediate-wet ($70^\circ < \theta < 110^\circ$) to weakly gas-wet ($110^\circ < \theta < 130^\circ$) as the TOC increased, which is consistent with previous studies using synthetically acid-aged shale samples.
7. The present work demonstrated a similarity in the H_2/brine and CH_4/brine wettability behavior by comparing the current study using the actual high TOC shale (13 to 18 wt%) to other studies providing a wide range of shale TOC from 0.1 to 20 wt%.

CRediT authorship contribution statement

Amer Alanazi: Conceptualization, Methodology, Investigation, Data curation, Software, Writing – original draft. **Nurudeen Yekeen:** Conceptualization, Formal analysis, Writing – review & editing. **Mujahid Ali:** Methodology, Investigation, Data curation, Validation, Software. **Muhammad Ali:** Methodology, Investigation, Data curation, Validation, Software. **Israa S. Abu-Mahfouz:** Visualization, Validation. **Alireza Keshavarz:** Validation, Resources, Project administration. **Stefan Iglauer:** Conceptualization, Visualization, Supervision. **Hussein Hoteit:** Conceptualization, Validation, Resources, Writing – review & editing, Supervision.

Declaration of competing interest

The authors declare that they have no known competing financial interests or personal relationships that could have appeared to influence the work reported in this paper.

Data availability

Data will be made available on request.

Acknowledgments

The authors acknowledge Karak International Oil (KIO) in Jordan, represented by Mr. Munther Akhroosh, for allowing core drilling in the Upper Cretaceous source rocks in KIO concession areas. The authors would like to thank the Ministry of Energy and Mineral Resources (MEMR) in Jordan for their continued support of our research projects. Additionally, we thank professor Khalil Khader (Hashemite University, Jordan) and Mr. Samer AlJurf for supervising the coring process. Finally, the authors acknowledge the King Abdullah University for Science and Technology (KAUST) and Edith Cowan University for providing the required infrastructure for this work.

Appendix A

The N_2 adsorption-desorption isotherms indicate a Type V isotherm following the work by Sing et al. (1985), attributed to the existence of mesopores with a weak interaction of N_2 on the pore surface (Garcia-Diego and Cuellar, 2005). The hysteresis in the N_2 adsorption-desorption isotherms for the four analyzed samples is relatively marginal at lower pressures (Fig. A.1). The hysteresis primarily depends on the mesoporous content and pore size. Specifically, N_2 molecules are first adsorbed on the walls of mesopores. Then, a film of the condensed adsorbed N_2 is made in the mesopores due to the depression effect of the saturated vapor pressure of confined N_2 (Andersson et al., 2018; Sing et al., 1985). Among all analyzed samples, Jordan-4 displayed the most significant hysteresis because of the diameter of the mesopores, which are near the critical diameter of N_2 at 77 K (around 4 nm; Abid et al., 2021). The pyrolysis profiles in the appendix (Figs. A.2 to A.5) indicate intermediate to high TOC values, ranging from 13 (Jordan-4) to 18 wt% (Jordan-1).

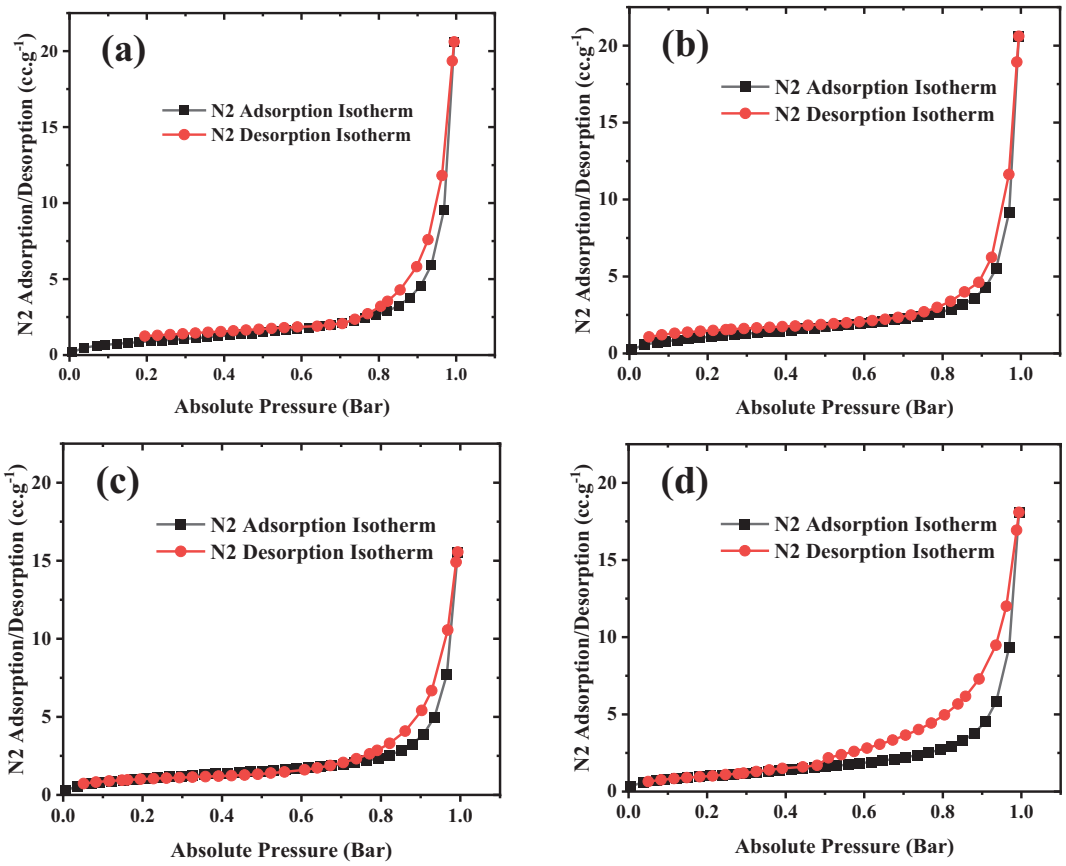

Fig. A.1. Nitrogen adsorption-desorption isotherm curves: a) Jordan-1, b) Jordan-2, c) Jordan-3, and d) Jordan-4.

The RockEval hydrocarbon pyrolysis indicates the TOC of the studied Jordanian oil shale samples depicted in Figs. A.2 to A.5.

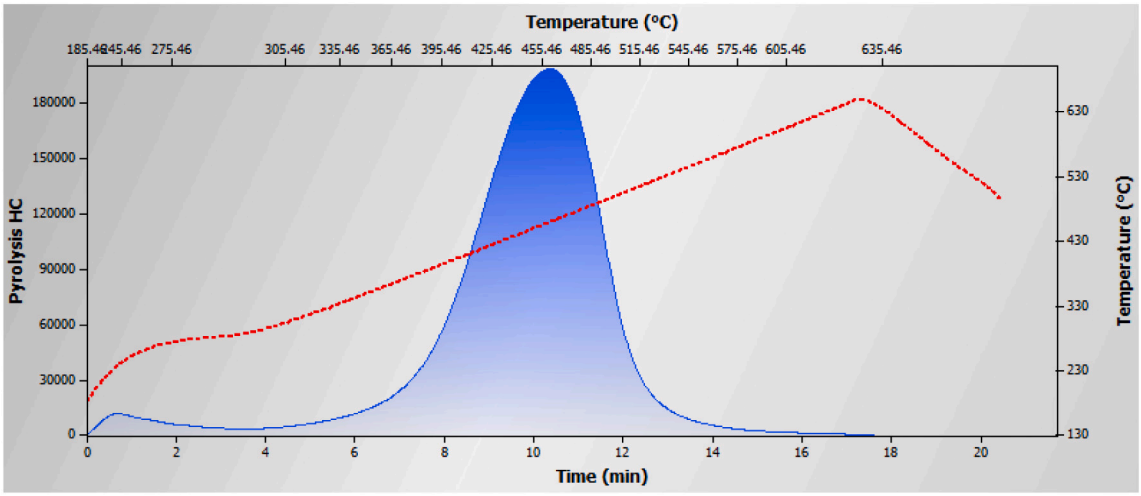

Fig. A.2. Hydrocarbon pyrolysis profile of Jordan-1 obtained from RockEval.

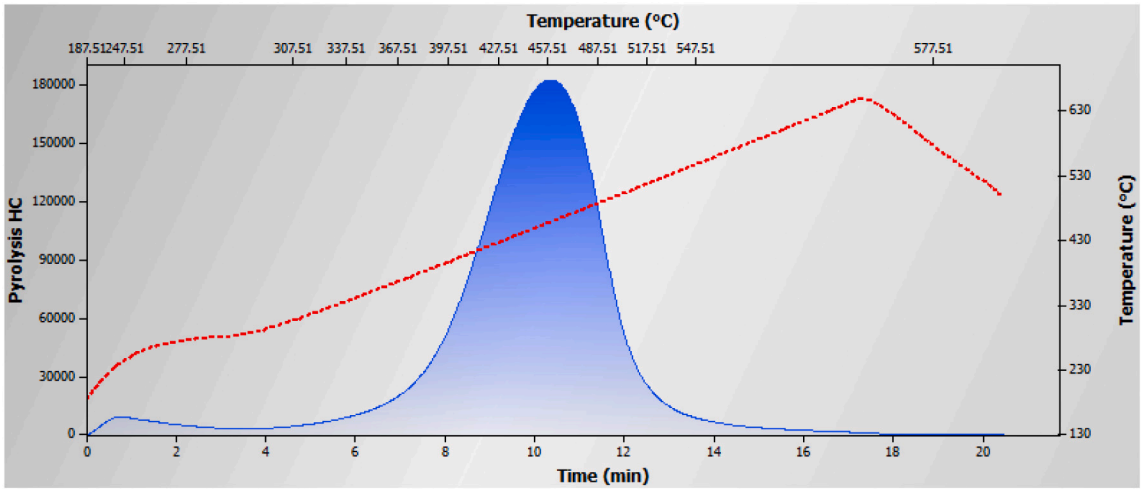

Fig. A.3. Hydrocarbon pyrolysis profile of Jordan-2 obtained from RockEval.

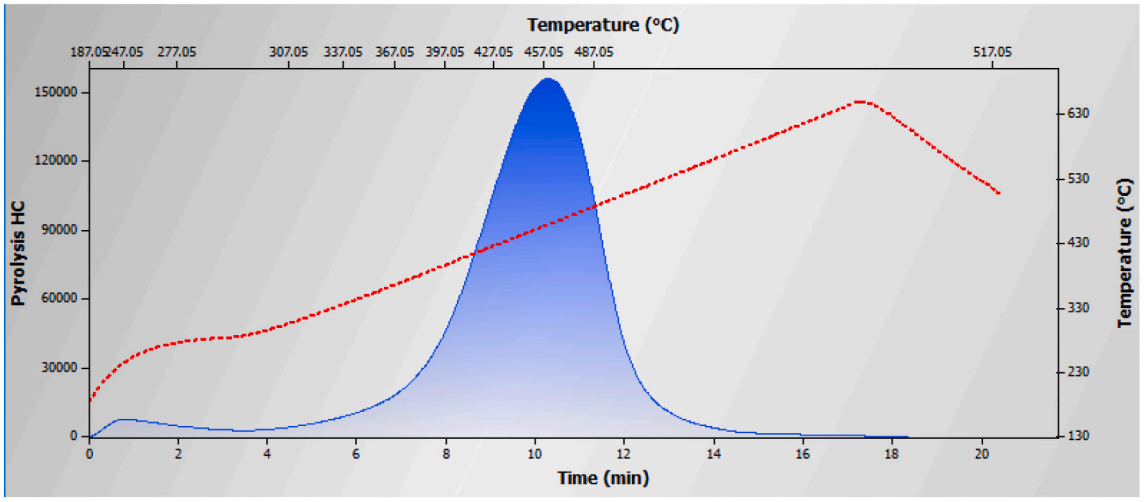

Fig. A.4. Hydrocarbon pyrolysis profile of Jordan-3 obtained from RockEval.

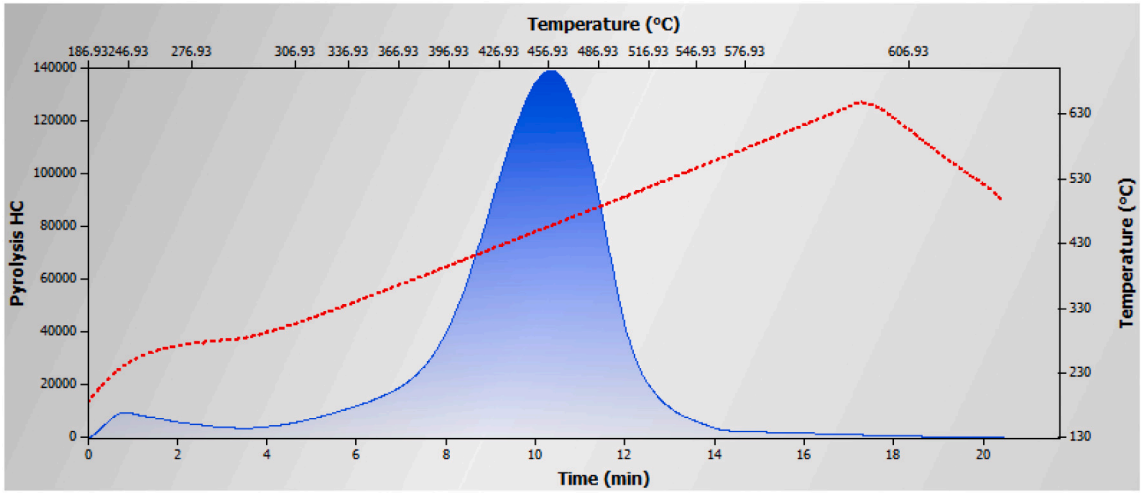

Fig. A.5. Hydrocarbon pyrolysis profile of Jordan-4 obtained from RockEval.

Table A.1
Contact angles of H_2, CH_4, and H_2-CH_4 mixtures on organic-rich shale source rocks at various pressures.

Rock sample	Gas type	Pressure, psi	Contact angle, degree	
			Advancing	Receding
Jordan-1	H_2	50	43	51
		400	54	64
		800	70	69
		1200	75	77
		1600	79	81
	CH_4	50	68	60
		400	87	77.8
		800	86	76
		1200	84	80
		1600	103	88
	H_2/CH_4	50	57	51
		400	65	64
		800	73	69
		1200	80	77
		1600	99	81
Jordan-2	H_2	50	52.7	54
		400	80	77.5
		800	86	78
		1200	98	94
		1600	97	89
	CH_4	50	87	74.2
		400	94	86.2
		800	99.6	88
		1200	107	96
		1600	110	92
	H_2/CH_4	50	73.8	67
		400	89	87
		800	92.6	87
		1200	102	95
		1600	105	91
Jordan-3	H_2	50	65	58
		400	85	68
		800	88	73
		1200	87	75
		1600	96	74
	CH_4	50	80	68
		400	98	87
		800	105	82
		1200	109	89
		1600	115	91
	H_2/CH_4	50	73	61
		400	92	79
		800	103	77
		1200	98	76
		1600	99	88
Jordan-4	H_2	50	63	38.2
		400	82	70
		800	86	67
		1200	92.6	78.3
		1600	106	81.4
	CH_4	50	75.7	71
		400	98	79
		800	114	91
		1200	112	105
		1600	122	103
	H_2/CH_4	50	71.9	64.4
		400	86	77
		800	91	88
		1200	101	89
		1600	111	102

References

[1] W. Fang, Z. Liu, A.R. Surya Putra, Role of research and development in green economic growth through renewable energy development: empirical evidence from South Asia, Renew. Energy 194 (2022) 1142–1152.

[2] U.S. Mohanty, M. Ali, M.R. Azhar, A. Al-Yaseri, A. Keshavarz, S. Iglauer, Current advances in syngas (CO+ H2) production through bi-reforming of methane using various catalysts: a review, Int. J. Hydrog. Energy 46 (65) (2021) 32809–32845.

[3] M. Ali, N.K. Jha, N. Pal, A. Keshavarz, H. Hoteit, M. Sarmadivaleh, Recent advances in carbon dioxide geological storage, experimental procedures, influencing parameters, and future outlook, Earth Sci. Rev. 225 (2022), 103895.

[4] M. Aslannezhad, M. Ali, A. Kalantariasl, M. Sayyafzadeh, Z. You, S. Iglauer, A. Keshavarz, A review of hydrogen/rock/brine interaction: implications for hydrogen geo-storage, Prog. Energy Combust. Sci. 95 (2023), 101066.

[5] M. Ali, Effect of Organic Surface Concentration on CO2-Wettability of Reservoir Rock, Curtin University, 2018.

[6] N. Yekeen, E. Padmanabhan, T.A.L. Sevoo, K.A.L. Kanesen, O.A. Okunade, Wettability of rock/CO2/brine systems: a critical review of influencing parameters and recent advances, J. Ind. Eng. Chem. 88 (2020) 1–28.

[7] F.J.F.M. Blunt Jr., F.M. Orr, Carbon dioxide in enhanced oil recovery, Energy Convers.Manag. 34 (1993) 9–11.

[8] O.C. Anika, S.G. Nnabuife, A. Bello, R.E. Okoroafor, B. Kuang, R. Villa, Prospects of low and zero-carbon renewable fuels in 1.5-degree net zero emission actualisation by 2050: a critical review, <sb:contribution><sb:title>Carbon Capture</sb:title></sb:contribution><sb:host><sb:issue><sb:series><sb:title>Sci. Technol.</sb:title></sb:series></sb:issue></sb:host> 100072 (2022).

[9] S. French, The role of zero and low carbon hydrogen in enabling the energy transition and the path to net zero greenhouse gas emissions: with global policies and demonstration projects hydrogen can play a role in a net zero future, Johnson Matthey Technol.Rev. 64 (3) (2020) 357–370.

[10] M. Bui, C.S. Adjiman, A. Bardow, E.J. Anthony, A. Boston, S. Brown, P.S. Fennell, S. Fuss, A. Galindo, L.A. Hackett, Carbon capture and storage (CCS): the way forward, Energy Environ. Sci. 11 (5) (2018) 1062–1176.

[11] A. Hassanpouryouzband, E. Joonaki, K. Edlmann, R.S. Haszeldine, Offshore geological storage of hydrogen: is this our best option to achieve net-zero? ACS Energy Lett. 6 (6) (2021) 2181–2186.

[12] A. Hassanpouryouzband, E. Joonaki, M.V. Farahani, S. Takeya, C. Ruppel, J. Yang, N.J. English, J.M. Schicks, K. Edlmann, H. Mehrabian, Gas hydrates in sustainable chemistry, Chem. Soc. Rev. 49 (15) (2020) 5225–5309.

[13] A.A. Mahesar, M. Ali, A.M. Shar, K.R. Memon, U.S. Mohanty, H. Akhondzadeh, A. H. Tunio, S. Iglauer, A. Keshavarz, Effect of cryogenic liquid nitrogen on the morphological and petrophysical characteristics of tight gas sandstone rocks from kirthar fold belt,Indus Basin, Pakistan, Energy Fuels 34 (11) (2020) 14548–14559.

[14] P. Balakrishnan, M.S. Shabbir, A.F. Siddiqi, X. Wang, Current status and future prospects of renewable energy: a case study, Energy Sources, Part A: Recov.Util. Environ.Eff. 42 (21) (2020) 2698–2703.

[15] D. Neupane, S. Kafle, K.R. Karki, D.H. Kim, P. Pradhan, Solar and wind energy potential assessment at provincial level in Nepal: geospatial and economic analysis, Renew. Energy 181 (2022) 278–291.

[16] A. Aftab, A. Hassanpouryouzband, Q. Xie, L.L. Machuca, M. Sarmadivaleh, Toward a fundamental understanding of geological hydrogen storage, Ind. Eng. Chem. Res. 61 (9) (2022) 3233–3253.

[17] A. Alanazi, M. Ali, S. Bawazeer, N. Yekeen, H. Hoteit, Evaluation of cubic, PC-SAFT, and GERG2008 equations of state for accurate calculations of thermophysical properties of hydrogen-blend mixtures, Energy Rep. 8 (2022) 13876–13899.

[18] N.S. Muhammed, B. Haq, D. Al Shehri, A. Al-Ahmed, M.M. Rahman, E. Zaman, A review on underground hydrogen storage: insight into geological sites, influencing factors and future outlook, Energy Rep. 8 (2022) 461–499.

[19] R. Tarkowski, B. Uliasz-Misiak, Towards underground hydrogen storage: a review of barriers, Renew. Sust. Energ. Rev. 162 (2022), 112451.

[20] D. Zivar, S. Kumar, J. Foroozesh, Underground hydrogen storage: a comprehensive review, Int. J. Hydrog. Energy 46 (45) (2021) 23436–23462.

[21] H.R. Abid, N. Yekeen, A. Al-Yaseri, A. Keshavarz, S. Iglauer, The impact of humic acid on hydrogen adsorptive capacity of eagle ford shale: implications for underground hydrogen storage, J.Energy Storage 55 (2022), 105615.

[22] A. Al-Yaseri, H. Al-Mukainah, N. Yekeen, A.S. Al-Qasim, Experimental investigation of hydrogen-carbonate reactions via computerized tomography: implications for underground hydrogen storage, Int. J. Hydrog. Energy 48 (9) (2023) 3583–3592.

[23] A. Alanazi, M. Ali, M. Mowafi, H. Hoteit, Effect of organics and nanofluids on capillary-sealing efficiency of caprock for hydrogen and carbon-dioxide geological storage, in: ARMA/DGS/SEG International Geomechanics Symposium, OnePetro, 2022.

[24] E.I. Epelle, W. Obande, G.A. Udourioh, I.C. Afolabi, K.S. Desongu, U. Orivri, B. Gunes, J.A. Okolie, Perspectives and prospects of underground hydrogen storage and natural hydrogen, Sustain.Energy Fuels 6 (14) (2022) 3324–3343.

[25] L. Zeng, A. Keshavarz, Q. Xie, S. Iglauer, Hydrogen storage in majiagou carbonate reservoir in China: geochemical modelling on carbonate dissolution and hydrogen loss, Int. J. Hydrog. Energy 47 (59) (2022) 24861–24870.

[26] L. Lankof, K. Urbańczyk, R. Tarkowski, Assessment of the potential for underground hydrogen storage in salt domes, Renew. Sust. Energ. Rev. 160 (2022), 112309.

[27] D. Grgic, F. Al Sahyouni, F. Golfier, M. Moumni, L. Schoumacker, Evolution of gas permeability of rock salt under different loading conditions and implications on the underground hydrogen storage in salt caverns, Rock Mech. Rock. Eng. 55 (2) (2022) 691–714.

[28] A. Małachowska, N. Łukasik, J. Mioduska, J. Gębicki, Hydrogen storage in geological formations—the potential of salt caverns, Energies 15 (14) (2022) 5038.

[29] M. Ali, N.K. Jha, A. Al-Yaseri, Y. Zhang, S. Iglauer, M. Sarmadivaleh, Hydrogen wettability of quartz substrates exposed to organic acids; implications for hydrogen trapping/storage in sandstone reservoirs, J. Pet. Sci. Eng. 207 (2021), 109081.

[30] M. Ali, B. Pan, N. Yekeen, S. Al-Anssari, A. Al-Anazi, A. Keshavarz, S. Iglauer, H. Hoteit, Assessment of wettability and rock-fluid interfacial tension of caprock: implications for hydrogen and carbon dioxide geo-storage, Int. J. Hydrog. Energy 47 (30) (2022) 14104–14120.

[31] M. Ali, F.U.R. Awan, M. Ali, A. Al-Yaseri, M. Arif, M. Sánchez-Román, A. Keshavarz, S. Iglauer, Effect of humic acid on CO2-wettability in sandstone formation, J. Colloid Interface Sci. 588 (2021) 315–325.

[32] F. Alhamad, M. Ali, M. Ali, H. Abid, H. Hoteit, S. Iglauer, A. Keshavarz, Effect of methyl orange on wettability of sandstone formations: implications for enhanced oil recovery, Energy Rep. 8 (2022) 12357–12365.

[33] L. Hashemi, M. Boon, W. Glerum, R. Farajzadeh, H. Hajibeygi, A comparative study for H2–CH4 mixture wettability in sandstone porous rocks relevant to underground hydrogen storage, Adv. Water Resour. 163 (2022), 104165.

[34] S.M.J. Raad, Y. Leonenko, H. Hassanzadeh, Hydrogen storage in saline aquifers: opportunities and challenges, Renew. Sust. Energ. Rev. 168 (2022), 112846.

[35] B. Pan, X. Yin, S. Iglauer, Rock-fluid interfacial tension at subsurface conditions: implications for H2, CO2 and natural gas geo-storage, Int. J. Hydrog. Energy 46 (50) (2021) 25578–25585.

[36] B. Pan, X. Yin, Y. Ju, S. Iglauer, Underground hydrogen storage: influencing parameters and future outlook, Adv. Colloid Interf. Sci. 294 (2021), 102473.

[37] S. Higgs, Y. Da Wang, C. Sun, J. Ennis-King, S.J. Jackson, R.T. Armstrong, P. Mostaghimi, In-situ hydrogen wettability characterisation for underground hydrogen storage, Int. J. Hydrog. Energy 47 (26) (2022) 13062–13075.

[38] H. Furukawa, O.M. Yaghi, Storage of hydrogen, methane, and carbon dioxide in highly porous covalent organic frameworks for clean energy applications, J. Am. Chem. Soc. 131 (25) (2009) 8875–8883.

[39] A. Alanazi, S. Bawazeer, M. Ali, A. Keshavarz, H. Hoteit, Thermodynamic modeling of hydrogen–water systems with gas impurity at various conditions using cubic and PC-SAFT equations of state, Energy Convers.Manag.X 15 (2022), 100257.

[40] E.R. Ugarte, S. Salehi, A review on well integrity issues for underground hydrogen storage, J.Energy Resour.Technol. 144 (4) (2021).

[41] M. Ghasemi, S. Omrani, S. Mahmoodpour, T. Zhou, Molecular dynamics simulation of hydrogen diffusion in water-saturated clay minerals; implications for underground hydrogen storage (UHS), Int. J. Hydrog. Energy 47 (59) (2022) 24871–24885.

[42] N. Yekeen, A. Al-Yaseri, B.M. Negash, M. Ali, A. Giwelli, L. Esteban, J. Sarout, Clay-hydrogen and clay-cushion gas interfacial tensions: implications for hydrogen storage, Int. J. Hydrog. Energy 47 (44) (2022) 19155–19167.

[43] V. Mirchi, M. Dejam, V. Alvarado, Interfacial tension and contact angle measurements for hydrogen-methane mixtures/brine/oil-wet rocks at reservoir conditions, Int. J. Hydrog. Energy 47 (82) (2022) 34963–34975.

[44] M. Hosseini, J. Fahimpour, M. Ali, A. Keshavarz, S. Iglauer, Hydrogen wettability of carbonate formations: implications for hydrogen geo-storage, J. Colloid Interface Sci. 614 (2022) 256–266.

[45] L. Zeng, M. Hosseini, A. Keshavarz, S. Iglauer, Y. Lu, Q. Xie, Hydrogen wettability in carbonate reservoirs: implication for underground hydrogen storage from geochemical perspective, Int. J. Hydrog. Energy 47 (60) (2022) 25357–25366.

[46] M. Ali, N.K. Jha, A. Al-Yaseri, Y. Zhang, S. Iglauer, M. Sarmadivaleh, Hydrogen wettability of quartz substrates exposed to organic acids;implications for hydrogen geo-storage in sandstone reservoirs, J. Pet. Sci. Eng. 207 (2021), 109081.

[47] A. Al-Yaseri, N.K. Jha, On hydrogen wettability of basaltic rock, J. Pet. Sci. Eng. 200 (2021), 108387.

[48] L. Hashemi, W. Glerum, R. Farajzadeh, H. Hajibeygi, Contact angle measurement for hydrogen/brine/sandstone system using captive-bubble method relevant for underground hydrogen storage, Adv. Water Resour. 154 (2021), 103964.

[49] M. Hosseini, J. Fahimpour, M. Ali, A. Keshavarz, S. Iglauer, H2− brine interfacial tension as a function of salinity, temperature, and pressure; implications for hydrogen geo-storage, J. Pet. Sci. Eng. 213 (2022), 110441.

[50] S. Iglauer, M. Ali, A. Keshavarz, Hydrogen wettability of sandstone reservoirs: implications for hydrogen geo-storage, Geophys. Res. Lett. 48 (3) (2021), e2020GL090814.

[51] M. Ali, B. Pan, N. Yekeen, S. Al-Anssari, A. Al-Anazi, A. Keshavarz, S. Iglauer, H. Hoteit, Assessment of wettability and rock-fluid interfacial tension of caprock: implications for hydrogen and carbon dioxide geo-storage, Int. J. Hydrog. Energy 47 (30) (2022) 14104–14120.

[52] A. Al-Yaseri, N. Yekeen, M. Ali, N. Pal, A. Verma, H. Abdulelah, H. Hoteit, M. Sarmadivaleh, Effect of organic acids on CO2-rock and water-rock interfacial tension: implications for CO2 geo-storage, J. Pet. Sci. Eng. 214 (2022), 110480.

[53] M. Ali, N. Yekeen, N. Pal, A. Keshavarz, S. Iglauer, H. Hoteit, Influence of pressure, temperature and organic surface concentration on hydrogen wettability of caprock; implications for hydrogen geo-storage, Energy Rep. 7 (2021) 5988–5996.

[54] H. Al-Mukainah, A. Al-Yaseri, N. Yekeen, J. Al Hamad, M. Mahmoud, Wettability of shale–brine–H2 system and H2-brine interfacial tension for assessment of the sealing capacities of shale formations during underground hydrogen storage, Energy Rep. 8 (2022) 8830–8843.

[55] M. Ali, N. Yekeen, N. Pal, A. Keshavarz, S. Iglauer, H. Hoteit, Influence of organic molecules on wetting characteristics of mica/H2/brine systems: implications for hydrogen structural trapping capacities, J. Colloid Interface Sci. 608 (2022) 1739–1749. Part 2.

[56] M. Hosseini, J. Fahimpour, M. Ali, A. Keshavarz, S. Iglauer, Capillary sealing efficiency analysis of caprocks: implication for hydrogen geological storage, Energy Fuel 36 (7) (2022) 4065–4075.

[57] M. Hosseini, M. Ali, J. Fahimpour, A. Keshavarz, S. Iglauer, Assessment of rock-hydrogen and rock-water interfacial tension in shale, evaporite and basaltic rocks, J.Nat.Gas Sci.Eng. 106 (2022), 104743.

[58] W. van Rooijen, L. Hashemi, M. Boon, R. Farajzadeh, H. Hajibeygi, Microfluidics-based analysis of dynamic contact angles relevant for underground hydrogen storage, Adv. Water Resour. 164 (2022), 104221.

[59] M. Ali, N. Yekeen, N. Pal, A. Keshavarz, S. Iglauer, H. Hoteit, Influence of organic molecules on wetting characteristics of mica/H2/brine systems: implications for hydrogen structural trapping capacities, J. Colloid Interface Sci. 608 (2) (2022) 1739–1749.

[60] S. Iglauer, H. Abid, A. Al-Yaseri, A. Keshavarz, Hydrogen adsorption on sub-bituminous coal: implications for hydrogen geo-storage, Geophys. Res. Lett. 48 (10) (2021), e2021GL092976.

[61] B. Pan, Y. Li, M. Zhang, X. Wang, S. Iglauer, Effect of total organic carbon (TOC) content on shale wettability at high pressure and high temperature conditions, J. Pet. Sci. Eng. 193 (2020), 107374.

[62] M. Arif, M. Lebedev, A. Barifcani, S. Iglauer, Influence of shale-total organic content on CO2 geo-storage potential, Geophys. Res. Lett. 44 (17) (2017) 8769–8775.

[63] T. Bakshi, V. Vishal, A review on the role of organic matter in gas adsorption in shale, Energy Fuel 35 (19) (2021) 15249–15264.

[64] M. Gasparik, P. Bertier, Y. Gensterblum, A. Ghanizadeh, B.M. Krooss, R. Littke, Geological controls on the methane storage capacity in organic-rich shales, Int. J. Coal Geol. 123 (2014) 34–51.

[65] H. Huang, R. Li, Z. Lyu, Y. Cheng, B. Zhao, Z. Jiang, Y. Zhang, F. Xiong, Comparative study of methane adsorption of middle-upper ordovician marine shales in the western Ordos Basin,NW China: insights into impacts of moisture on thermodynamics and kinetics of adsorption, Chem. Eng. J. 446 (2022), 137411.

[66] L. Ji, T. Zhang, K.L. Milliken, J. Qu, X. Zhang, Experimental investigation of main controls to methane adsorption in clay-rich rocks, Appl. Geochem. 27 (12) (2012) 2533–2545.

[67] M. Shabani, S.A. Moallemi, B.M. Krooss, A. Amann-Hildenbrand, Z. Zamani-Pozveh, H. Ghalavand, R. Littke, Methane sorption and storage characteristics of organic-rich carbonaceous rocks, Lurestan province, southwest Iran, Int. J. Coal Geol. 186 (2018) 51–64.

[68] T. Zhang, G.S. Ellis, S.C. Ruppel, K. Milliken, R. Yang, Effect of organic-matter type and thermal maturity on methane adsorption in shale-gas systems, Org. Geochem. 47 (2012) 120–131.

[69] S. Higgs, Y. Da Wang, C. Sun, J. Ennis-King, S.J. Jackson, R.T. Armstrong, P. Mostaghimi, In-situ hydrogen wettability characterisation for underground hydrogen storage, Int. J. Hydrog. Energy 47 (26) (2022) 13062–13075.

[70] R. Sedev, H. Akhondzadeh, M. Ali, A. Keshavarz, S. Iglauer, Contact angles of a brine on a bituminous coal in compressed hydrogen, Geophys. Res. Lett. 49 (8) (2022), e2022GL098261.

[71] A. Alanazi, M.Al Malallah, M. Mowafi, W. Badeghaish, H. Hoteit, A. Al-Yaseri, J. Al-Hamad, Hydrogen wettability measurement of Saudi basaltic rocks at underground storage conditions, in: International Geomechanics Symposium, OnePetro, 2022.

[72] A. Al-Yaseri, D. Wolff-Boenisch, C.A. Fauziah, S. Iglauer, Hydrogen wettability of clays: implications for underground hydrogen storage, Int. J. Hydrog. Energy 46 (69) (2021) 34356–34361.

[73] A. Al-Yaseri, N. Yekeen, M. Mahmoud, A. Kakati, Q. Xie, A. Giwelli, Thermodynamic characterization of H2-brine-shale wettability: implications for hydrogen storage at subsurface, Int. J. Hydrog. Energy 47 (53) (2022) 22510–22521.

[74] M. Boon, H. Hajibeygi, Experimental characterization of H 2/water multiphase flow in heterogeneous sandstone rock at the core scale relevant for underground hydrogen storage (UHS), Sci. Rep. 12 (1) (2022) 14604.

[75] W. van Rooijen, L. Hashemi, M. Boon, R. Farajzadeh, H. Hajibeygi, Microfluidics-based analysis of dynamic contact angles relevant for underground hydrogen storage, Adv. Water Resour. 104221 (2022).

[76] L. Zeng, A. Keshavarz, N.K. Jha, A. Al-Yaseri, M. Sarmadivaleh, Q. Xie, S. Iglauer, Geochemical modelling of hydrogen wettability on quartz: implications for underground hydrogen storage in sandstone reservoirs, J. Mol. Liq. 371 (2023), 121076.

[77] M. Alqudah, M. Ali Hussein, S. van den Boorn, O.G. Podlaha, J. Mutterlose, Biostratigraphy and depositional setting of Maastrichtian – Eocene oil shales from Jordan, Mar. Pet. Geol. 60 (2015) 87–104.

[78] M.H. Hakimi, W.H. Abdullah, M. Alqudah, Y.M. Makeen, K.A. Mustapha, Organic geochemical and petrographic characteristics of the oil shales in the Lajjun area, central Jordan: origin of organic matter input and preservation conditions, Fuel 181 (2016) 34–45.

[79] J.H. Powell, B.K. Moh'd, Evolution of Cretaceous to Eocene alluvial and carbonate platform sequences in central and south Jordan, GeoArabia 16 (4) (2011) 29–82.

[80] I.S. Abu-Mahfouz, J.A. Cartwright, E. Idiz, J.N. Hooker, S. Robinson, S. van den Boorn, Genesis and role of bitumen in fracture development during early catagenesis, Pet. Geosci. 25 (4) (2019) 371–388.

[81] P. Eskelinen, X-ray diffraction study of TiO2 thin films on mica, J. Solid State Chem. 100 (2) (1992) 356–362.

[82] J.D. Rodriguez-Blanco, S. Shaw, L.G. Benning, The kinetics and mechanisms of amorphous calcium carbonate (ACC) crystallization to calcite, viavaterite, Nanoscale 3 (1) (2011) 265–271.

[83] F. Andersen, L. Brecevic, ChemInform abstract: infrared spectra of amorphous and crystalline calcium carbonate, ChemInform 23 (2010) no-no.

[84] J. Kiefer, A. Stärk, A.L. Kiefer, H. Glade, Infrared spectroscopic analysis of the inorganic deposits from water in domestic and technical heat exchangers, Energies 11 (4) (2018) 798.

[85] J. Ji, Y. Ge, W. Balsam, J.E. Damuth, J. Chen, Rapid identification of dolomite using a Fourier transform infrared spectrophotometer (FTIR): a fast method for identifying Heinrich events in IODP Site U1308, Mar. Geol. 258 (1) (2009) 60–68.

[86] D. Chakrabarty, S. Mahapatra, Aragonite crystals with unconventional morphologies, J. Mater. Chem. 9 (11) (1999) 2953–2957.

[87] X. Wang, Y. Ye, X. Wu, J.R. Smyth, Y. Yang, Z. Zhang, Z. Wang, High-temperature Raman and FTIR study of aragonite-group carbonates, Phys. Chem. Miner. 46 (1) (2019) 51–62.

[88] J. Coates Interpretation of Infrared Spectra, A Practical Approach, Encyclopedia of Analytical Chemistry.

[89] A.B.D. Nandiyanto, R. Oktiani, R. Ragadhita, in: How to Read and Interpret FTIR Spectroscope of Organic Material, 2019 4(1), 2019, p. 22.

[90] K.M. George, T.C. Ruthenburg, J. Smith, L. Yu, Q. Zhang, C. Anastasio, A. M. Dillner, FT-IR quantification of the carbonyl functional group in aqueous-phase secondary organic aerosol from phenols, Atmos. Environ. 100 (2015) 230–237.

[91] O.A. Okunade, N. Yekeen, E. Padmanabhan, A. Al-Yaseri, A.K. Idris, J.A. Khan, Shale core wettability alteration, foam and emulsion stabilization by surfactant: impact of surfactant concentration, rock surface roughness and nanoparticles, J. Pet. Sci. Eng. 207 (2021), 109139.

[92] A. Marmur, Soft contact: measurement and interpretation of contact angles, Soft Matter 2 (1) (2006) 12–17.

[93] A.Z. Al-Yaseri, M. Lebedev, A. Barifcani, S. Iglauer, Receding and advancing (CO2 + brine+ quartz) contact angles as a function of pressure, temperature, surface roughness, salt type and salinity, J. Chem. Thermodyn. 93 (2016) 416–423.

[94] L.M. Lander, L.M. Siewierski, W.J. Brittain, E.A. Vogler, A systematic comparison of contact angle methods, Langmuir 9 (8) (1993) 2237–2239.

[95] E.A. Al-Khdheeawi, S. Vialle, A. Barifcani, M. Sarmadivaleh, S. Iglauer, Impact of reservoir wettability and heterogeneity on CO2-plume migration and trapping capacity, Int. J. Greenhouse Gas Control 58 (2017) 142–158.

[96] E.A. Al-Khdheeawi, S. Vialle, A. Barifcani, M. Sarmadivaleh, S. Iglauer, Influence of injection well configuration and rock wettability on CO2 plume behaviour and CO2 trapping capacity in heterogeneous reservoirs, J.Nat.Gas Sci.Eng. 43 (2017) 190–206.

[97] S. Al-Anssari, Z.-U.-A. Arain, H.A. Shanshool, M. Ali, A. Keshavarz, S. Iglauer, M. Sarmadivaleh, Effect of Nanoparticles on the Interfacial Tension of CO-Oil System at High Pressure and Temperature: An Experimental Approach, SPE Asia Pacific Oil & Gas Conference and Exhibition, Society of Petroleum Engineers, 2020.

[98] S. Iglauer, A.Z. Al-Yaseri, R. Rezaee, M. Lebedev, CO2 wettability of caprocks: implications for structural storage capacity and containment security, Geophys. Res. Lett. 42 (21) (2015) 9279–9284.

[99] S. Iglauer, C. Pentland, A. Busch, CO2 wettability of seal and reservoir rocks and the implications for carbon geo-sequestration, Water Resour. Res. 51 (1) (2015) 729–774.

[100] S. Iglauer, CO2–water–rock wettability: variability, influencing factors, and implications for CO2 geostorage, Acc. Chem. Res. 50 (5) (2017) 1134–1142.

[101] M. Ali, N.U. Dahraj, S.A. Haider, Study of asphaltene precipitation during CO2 injection in light oil reservoirs, in: SPE/PAPG Pakistan Section Annual Technical Conference, Society of Petroleum Engineers, 2015.

[102] M. Arif, A. Barifcani, M. Lebedev, S. Iglauer, Structural trapping capacity of oil-wet caprock as a function of pressure, temperature and salinity, Int. J. Greenhouse Gas Control 50 (2016) 112–120.

[103] A. Al-Yaseri, N.K. Jha, On hydrogen wettability of basaltic rock, J. Pet. Sci. Eng. 108387 (2021).

[104] S. Iglauer, M. Ali, A. Keshavarz, Hydrogen wettability of sandstone reservoirs: implications for hydrogen geo-storage, Geophys. Res. Lett. 48 (3) (2021) 1–5.

[105] N.K. Jha, A. Al-Yaseri, M. Ghasemi, D. Al-Bayati, M. Lebedev, M. Sarmadivaleh, Pore scale investigation of hydrogen injection in sandstone via X-ray micro-tomography, Int. J. Hydrog. Energy 46 (70) (2021) 34822–34829.

[106] N.K. Jha, M. Lebedev, S. Iglauer, M. Ali, H. Roshan, A. Barifcani, J.S. Sangwai, M. Sarmadivaleh, Pore scale investigation of low salinity surfactant nanofluid injection into oil saturated sandstone via X-ray micro-tomography, J. Colloid Interface Sci. 562 (2020) 370–380.

[107] M. Ali, A. Aftab, F.U.R. Awan, H. Akhondzadeh, A. Keshavarz, A. Saeedi, S. Iglauer, M. Sarmadivaleh, CO2-wettability reversal of cap-rock by alumina nanofluid: implications for CO2 geo-storage, Fuel Process. Technol. 214 (2021), 106722.

[108] N. Jha, M. Ali, M. Sarmadivaleh, S. Iglauer, A. Barifcani, M. Lebedev, J. Sangwai, Low salinity surfactant nanofluids for enhanced CO2 storage application at high pressure and temperature, in: Fifth CO2 Geological Storage Workshop, European Association of Geoscientists & Engineers, 2018, pp. 1–4.

[109] N.K. Jha, M. Ali, S. Iglauer, M. Lebedev, H. Roshan, A. Barifcani, J.S. Sangwai, M. Sarmadivaleh, Wettability alteration of quartz surface by low-salinity surfactant nanofluids at high-pressure and high-temperature conditions, Energy Fuel 33 (8) (2019) 7062–7068.

[110] D. Broseta, N. Tonnet, V. Shah, Are rocks still water-wet in the presence of dense CO2 or H2S? Geofluids 12 (4) (2012) 280–294.

[111] A.S. Al-Menhali, S. Krevor, Capillary trapping of CO2 in oil reservoirs: observations in a mixed-wet carbonate rock, Environ.Sci.Technol. 50 (5) (2016) 2727–2734.

[112] P. Chiquet, D. Broseta, S. Thibeau, Wettability alteration of caprock minerals by carbon dioxide, Geofluids 7 (2) (2007) 112–122.

[113] T. Rahman, M. Lebedev, A. Barifcani, S. Iglauer, Residual trapping of supercritical CO2 in oil-wet sandstone, J. Colloid Interface Sci. 469 (2016) 63–68.

[114] D.M. Akob, I.M. Cozzarelli, D.S. Dunlap, E.L. Rowan, M.M. Lorah, Organic and inorganic composition and microbiology of produced waters from Pennsylvania shale gas wells, Appl. Geochem. 60 (2015) 116–125.
[115] P.D. Lundegard, Y.K. Kharaka, Distribution and occurrence of organic acids in subsurface waters, in: Organic Acids in Geological Processes, Springer, 1994, pp. 40–69.
[116] B. Caballero, L.C. Trugo, P.M. Finglas, Encyclopedia of Food Sciences and Nutrition, Academic, 2003.
[117] M. Arif, S.A. Abu-Khamsin, S. Iglauer, Wettability of rock/CO2/brine and rock/oil/CO2-enriched-brine systems: critical parametric analysis and future outlook, Adv. Colloid Interf. Sci. 268 (2019) 91–113.
[118] S. Al-Anssari, Z.-U.-A. Arain, A. Barifcani, A. Keshavarz, M. Ali, S. Iglauer, Influence of pressure and temperature on CO2-nanofluid interfacial tension: implication for enhanced oil recovery and carbon geosequestration, in: Abu Dhabi International Petroleum Exhibition & Conference, 2018.
[119] S. Al-Anssari, Z.-U.-A. Arain, H.A. Shanshool, M. Ali, A. Keshavarz, S. Iglauer, M. Sarmadivaleh, Effect of nanoparticles on the interfacial tension of CO2-oil system at high pressure and temperature: an experimental approach, in: SPE Asia Pacific Oil & Gas Conference and Exhibition, 2020.
[120] S. Iglauer, W. Wülling, C.H. Pentland, S.K. Al-Mansoori, M.J. Blunt, Capillary-trapping capacity of sandstones and sandpacks, SPE J. 16 (04) (2011) 778–783.
[121] M. Hosseini, J. Fahimpour, M. Ali, A. Keshavarz, S. Iglauer, Capillary sealing efficiency analysis of caprocks: implication for hydrogen geological storage, Energy Fuel 36 (7) (2022) 4065–4075.
[122] M. Ali, A. Aftab, Z.-U.-A. Arain, A. Al-Yaseri, H. Roshan, A. Saeedi, S. Iglauer, M. Sarmadivaleh, Influence of organic acid concentration on wettability alteration of cap-rock: implications for CO2 trapping/storage, ACS Appl. Mater. Interfaces 12 (35) (2020) 39850–39858.
[123] M. Ali, S. Al-Anssari, M. Arif, A. Barifcani, M. Sarmadivaleh, L. Stalker, M. Lebedev, S. Iglauer, Organic acid concentration thresholds for ageing of carbonate minerals: implications for CO2 trapping/storage, J. Colloid Interface Sci. 534 (2019) 88–94.
[124] M. Ali, M. Arif, M.F. Sahito, S. Al-Anssari, A. Keshavarz, A. Barifcani, L. Stalker, M. Sarmadivaleh, S. Iglauer, CO2-wettability of sandstones exposed to traces of organic acids: implications for CO2 geo-storage, Int. J. Greenhouse Gas Control 83 (2019) 61–68.
[125] M. Hosseini, J. Fahimpour, M. Ali, A. Keshavarz, S. Iglauer, H2– brine interfacial tension as a function of salinity, temperature, and pressure; implications for hydrogen geo-storage, J. Pet. Sci. Eng. 110441 (2022).
[126] E.W. Lemmon, I.H. Bell, M. Huber, M. McLinden, NIST Standard Reference Database 23: Reference Fluid Thermodynamic and Transport Properties-REFPROP, Version 10.0, National Institute of Standards and Technology, Standard Reference Data Program, Gaithersburg, 2018.
[127] M. Hosseini, J. Fahimpour, M. Ali, A. Keshavarz, S. Iglauer, Hydrogen wettability of carbonate formations: implications for hydrogen geo-storage, J. Colloid Interface Sci. 614 (2022) 256–266.
[128] A. Abramov, A. Keshavarz, S. Iglauer, Wettability of fully hydroxylated and alkylated (001) α-quartz surface in carbon dioxide atmosphere, J. Phys. Chem. C 123 (14) (2019) 9027–9040.
[129] A. Al-Yaseri, H. Abdulelah, N. Yekeen, M. Ali, B.M. Negash, Y. Zhang, Assessment of CO2/shale interfacial tension, Colloids Surf. A Physicochem. Eng. Asp. 627 (2021), 127118.
[130] N.S. Kaveh, A. Barnhoorn, K.-H. Wolf, Wettability evaluation of silty shale caprocks for CO2 storage, Int. J. Greenhouse Gas Control 49 (2016) 425–435.
[131] M. Ali, Effect of Organics and Nanoparticles on CO2-Wettability of Reservoir Rock; Implications for CO2 Geo-Storage, Curtin University, 2021.
[132] M. Ali, N. Yekeen, M. Ali, M. Hosseini, N. Pal, A. Keshavarz, S. Iglauer, H. Hoteit, Effects of various solvents on adsorption of organics for porous and nonporous quartz/CO2: implications for CO2 geo-storage, Energy Fuel 36 (18) (2022) 11089–11099.
[133] A. Al-Yaseri, N. Yekeen, M. Ali, N. Pal, A. Verma, H. Abdulelah, H. Hoteit, M. Sarmadivaleh, Effect of organic acids on CO2-rock and water-rock interfacial tension: implications for CO2 geo-storage, J. Pet. Sci. Eng. 110480 (2022).
[134] M. Alshakhs, M.R. Rezaee, A new method to estimate total organic carbon (TOC) content, an example from Goldwyer Shale Formation, the Canning Basin, <sb:contribution><sb:title>Open Pet. </sb:title></sb:contribution><sb:host><sb:issue><sb:series><sb:title><sb:maintitle>Eng. J.</sb:maintitle> </sb:title></sb:series></sb:issue></sb:host> 10 (2017) 118–133.
[135] W. Orem, C. Tatu, M. Varonka, H. Lerch, A. Bates, M. Engle, L. Crosby, J. McIntosh, Organic substances in produced and formation water from unconventional natural gas extraction in coal and shale, Int. J. Coal Geol. 126 (2014) 20–31.
[136] I. Gupta, J. Jernigen, M. Curtis, C. Rai, C. Sondergeld, Water-wet or oil-wet: is it really that simple in shales? Petrophysics SPWLA J. Form. Eval. Reserv. Description 59 (03) (2018) 308–317.
[137] Q. Lan, M. Xu, M. Binazadeh, H. Dehghanpour, J.M. Wood, A comparative investigation of shale wettability: the significance of pore connectivity, J.Nat.Gas Sci.Eng. 27 (2015) 1174–1188.
[138] M.R. Yassin, M. Begum, H. Dehghanpour, Organic shale wettability and its relationship to other petrophysical properties: a duvernay case study, Int. J. Coal Geol. 169 (2017) 74–91.
[139] M. Arif, A. Barifcani, M. Lebedev, S. Iglauer, CO2-wettability of low to high rank coal seams: implications for carbon sequestration and enhanced methane recovery, Fuel 181 (2016) 680–689.
[140] D.N. Espinoza, J.C. Santamarina, CO2 breakthrough—caprock sealing efficiency and integrity for carbon geological storage, Int. J. Greenhouse Gas Control 66 (2017) 218–229.
[141] H. Esfandyari, M. Sarmadivaleh, F. Esmaeilzadeh, M. Ali, S. Iglauer, A. Keshavarz, Experimental evaluation of rock mineralogy on hydrogen-wettability: implications for hydrogen geo-storage, J.Energy Storage 52 (2022), 104866.
[142] S. Iglauer, H. Akhondzadeh, H. Abid, A. Paluszny, A. Keshavarz, M. Ali, A. Giwelli, L. Esteban, J. Sarout, M. Lebedev, Hydrogen flooding of a coal core: effect on coal swelling, Geophys. Res. Lett. 49 (6) (2022), e2021GL096873.
[143] A. Keshavarz, H. Abid, M. Ali, S. Iglauer, Hydrogen diffusion in coal: implications for hydrogen geo-storage, J. Colloid Interface Sci. 608 (2022) 1457–1462.
[144] A. Al-Yaseri, L. Esteban, A. Giwelli, J. Sarout, M. Lebedev, M. Sarmadivaleh, Initial and residual trapping of hydrogen and nitrogen in Fontainebleau sandstone using nuclear magnetic resonance core flooding, Int. J. Hydrog. Energy 47 (53) (2022) 22482–22494.